



European Research Community On Flow, Turbulence and Combustion

ERCOFTAC is a leading European association of research, education and industry groups in the technology of flow, turbulence and combustion. The main objectives of ERCOFTAC are: To promote joint efforts of European research institutes and industries with the aim of **exchanging technical and scientific information**; to promote **Pilot Centres** for collaboration, stimulation and

application of research across Europe; to stimulate, through the creation of **Special Interest Groups**, well-coordinated European-wide research efforts on specific topics; to stimulate the creation of advanced training activities; and to be influential on funding agencies, governments, the European Commission and the European Parliament.

www.ercoftac.org

Honorary Presidents

Mathieu, J. Spalding, D.B.

Executive Committee

Chairman Hutton, A.G.
Airbus UK
Building 09B
Bristol BS99 7AR
United Kingdom
Tel: +44 117 936 7519
anthony.hutton@airbus.com

Deputy Chairman Tomboulides, A.
Deputy Chairman Hirsch, C.
Treasurer Duursma, R.P.J.
Deputy Treasurer Ooms, G.
SPC Chairman Geurts, B.J.
SPC Deputy Chairman Von Terzi, D.
IPC Chairman Geuzaine, P.
SPC Deputy Chairman Oliemans, R.V.A.
Horizon 10 Chairman Jakirlic, S.
Ind. Engagement Officer Seoud, R.E.
Knowledge Base Editor Rodi, W.
Observer Hunt, J.
Observer Jacquin, L.
Secretary Borhani, N.

ERCOFTAC Administration and Development Office

Director Hirsch, C.
ERCOFTAC ADO
Numeca International
Chaussée de la Hulpe 189
Terhulpesteenweg
B-1170 Brussels
Belgium
Tel: +32 2 643 3572
Fax: +32 2 647 9398
ado@ercoftac.be

Webmaster Babayan, A.
webmaster@ercoftac.be

Secretary Laurent, A.
anne.laurent@numeca.be

Scientific Programme Committee

Chairman Geurts, B.J.
University of Twente
Mathematical Sciences
PO Box 217
NL-7500 AE Enschede
The Netherlands
Tel: +31 53 489 4125
b.j.geurts@utwente.nl

Deputy Chairman Von Terzi, D.

Industrial Programme Committee

Chairman Geuzaine, P.

Deputy Chairman Oliemans, R.V.A.

Engagement Officer Seoud, R.E.
21 Ashbourne Terrace
Wimbeldon SW19 1QX
United Kingdom
Tel: +44 208 543 9343
richard.seoud-ieo@ercoftac.org

ERCOFTAC Coordination Centre

Director Thome, J.R.

Secretary Borhani, N.
ERCOFTAC Coordination Centre
Laboratory of Heat and Mass Transfer
EPFL-STI-IGM-ERCOFTAC
ME G1 465, Station 9
CH-1015 Lausanne VD
Switzerland
Tel: +41 21 693 3503
Fax: +41 21 693 5960
ercoftac@epfl.

TABLE OF CONTENTS

SPECIAL THEME

'Fibre Suspension Flows'

Editorial - Fibre Suspension Flows <i>F. Lundell and J. Hämäläinen</i>	3
DNS of Non-Spherical Particles in Turbulent Flows <i>H.I. Andersson and L. Zhao</i>	4
Electrical Resistance Tomography Technique in Pulp and Paper Industry <i>L. Heikkinen, J. Kourunen, P. Paananen, K. Peltonen, J. Käyhkö and M. Vauhkonen</i>	9
On the Flow Behaviour of Wood Fibre Suspensions <i>A. Jäsberg</i>	12
Fibre Suspension Rheology Research at VTT <i>A. Koponen</i>	14
Streak Formation and Fibre Orientation in Near Wall Turbulent Fibre Suspension Flow <i>M. Kvick, K. Hakansson, F. Lundell, L.D. Söderberg and L. Prah Wittberg</i>	19
Eulerian Approach to Model Fibre Orientation and Fibre Flocculation in Papermaking <i>H. Niskanen, T. Hämäläinen and J. Hämäläinen</i>	23
Orientation of Fibers in Different Contraction Profiles <i>M. Putkiranta, H. Eloranta, T. Pärssinen T. and P. Saarenrinne</i>	27
Modelling Fibre Suspension Flow Using a Continuum Approach Experimental Characterization and Simulation <i>M.G. Rasteiro, F.A.P. Garcia, P.J. Ferreira and C.A.F. Ventura</i>	30

EDITOR	Borhani, N.
CHAIRMAN	Elsner, W.
EDITORIAL BOARD	Armenio, V. Dick, E. Geurts, B.J.
DESIGN & LAYOUT	Borhani, N. Nichita, B.A.

SUBMISSIONS

ERCOFTAC Bulletin
ERCOFTAC Coordination Centre
Laboratory of Heat and Mass Transfer
EPFL-STI-IGM-ERCOFTAC
ME G1 465, Station 9
CH-1015 Lausanne VD
Switzerland

Tel: +41 21 693 3503
Fax: +41 21 693 5960
Email: ercoftac@epfl.ch

HOSTED, PRINTED & DISTRIBUTED BY



ÉCOLE POLYTECHNIQUE
FÉDÉRALE DE LAUSANNE

The reader should note that the Editorial Board cannot accept responsibility for the accuracy of statements made by any contributing authors

NEXT ERCOFTAC EVENTS

ERCOFTAC Spring Festival

12th May 2011

Polish Academy of Sciences, Gdansk, Poland.

ERCOFTAC SPC, IPC & EC Meetings

13th May 2011

Polish Academy of Sciences, Gdansk, Poland.



The ERCOFTAC Best Practice Guidelines for Industrial Computational Fluid Dynamics

The Best Practice Guidelines (BPG) were commissioned by ERCOFTAC following an extensive consultation with European industry which revealed an urgent demand for such a document. The first edition was completed in January 2000 and constitutes generic advice on how to carry out quality CFD calculations. The BPG therefore address mesh design; construction of numerical boundary conditions where problem data is uncertain; mesh and model sensitivity checks; distinction between numerical and turbulence model inadequacy; preliminary information regarding the limitations of turbulence models etc. The aim is to encourage a common best practice by virtue of which separate analyses of the same problem, using the same model physics, should produce consistent results. Input and advice was sought from a wide cross-section of CFD specialists, eminent academics, end-users and, (particularly important) the leading commercial code vendors established in Europe. Thus, the final document can be considered to represent the consensus view of the European CFD community.

Inevitably, the Guidelines cannot cover every aspect of CFD in detail. They are intended to offer roughly those 20% of the most important general rules of advice that cover roughly 80% of the problems likely to be encountered. As such, they constitute essential information for the novice user and provide a basis for quality management and regulation of safety submissions which rely on CFD. Experience has also shown that they can often provide useful advice for the more experienced user. The technical content is limited to single-phase, compressible and incompressible, steady and unsteady, turbulent and laminar flow with and without heat transfer. Versions which are customised to other aspects of CFD (the remaining 20% of problems) are planned for the future.

The seven principle chapters of the document address numerical, convergence and round-off errors; turbulence modelling; application uncertainties; user errors; code errors; validation and sensitivity tests for CFD models and finally examples of the BPG applied in practice. In the first six of these, each of the different sources of error and uncertainty are examined and discussed, including references to important books, articles and reviews. Following the discussion sections, short simple bullet-point statements of advice are listed which provide clear guidance and are easily understandable without elaborate mathematics. As an illustrative example, an extract dealing with the use of turbulent wall functions is given below:

- Check that the correct form of the wall function is being used to take into account the wall roughness. An equivalent roughness height and a modified multiplier in the law of the wall must be used.
- Check the upper limit on y^+ . In the case of moderate Reynolds number, where the boundary layer only extends to y^+ of 300 to 500, there is no chance of accurately resolving the boundary layer if the first integration point is placed at a location with the value of y^+ of 100.

- Check the lower limit of y^+ . In the commonly used applications of wall functions, the meshing should be arranged so that the values of y^+ at all the wall-adjacent integration points is only slightly above the recommended lower limit given by the code developers, typically between 20 and 30 (the form usually assumed for the wall functions is not valid much below these values). This procedure offers the best chances to resolve the turbulent portion of the boundary layer. It should be noted that this criterion is impossible to satisfy close to separation or reattachment zones unless y^+ is based upon y^* .
- Exercise care when calculating the flow using different schemes or different codes with wall functions on the same mesh. Cell centred schemes have their integration points at different locations in a mesh cell than cell vertex schemes. Thus the y^+ value associated with a wall-adjacent cell differs according to which scheme is being used on the mesh.
- Check the resolution of the boundary layer. If boundary layer effects are important, it is recommended that the resolution of the boundary layer is checked after the computation. This can be achieved by a plot of the ratio between the turbulent to the molecular viscosity, which is high inside the boundary layer. Adequate boundary layer resolution requires at least 8-10 points in the layer.

All such statements of advice are gathered together at the end of the document to provide a 'Best Practice Checklist'. The examples chapter provides detailed expositions of eight test cases each one calculated by a code vendor (viz FLUENT, AEA Technology, Computational Dynamics, NUMECA) or code developer (viz Electricité de France, CEA, British Energy) and each of which highlights one or more specific points of advice arising in the BPG. These test cases range from natural convection in a cavity through to flow in a low speed centrifugal compressor and in an internal combustion engine valve.

Copies of the Best Practice Guidelines can be acquired from:

ERCOFTAC ADO
Chaussée de la Hulpe 187-189
B-1170 Brussels
Belgium
Tel: +32 2 643 3572
Fax: +32 2 647 9398
Email: emilie.jean@numeca.be

The price per copy (not including postage) is:

Non-ERCOFTAC members: 150 Euros
Non-ERCOFTAC academics: 75 Euros

ERCOFTAC members: 100 Euros
ERCOFTAC academic members: 50 Euros

SPECIAL THEME

FIBRE SUSPENSION FLOWS

Fredrik Lundell¹ & Jari Hämäläinen²

¹*Linné FLOW Centre and Wallenberg Wood Science Centre, KTH Mechanics, Royal Institute of Technology, Sweden.*

²*Department of Physics and Mathematics University of Eastern Finland, Kuopio, Finland.*

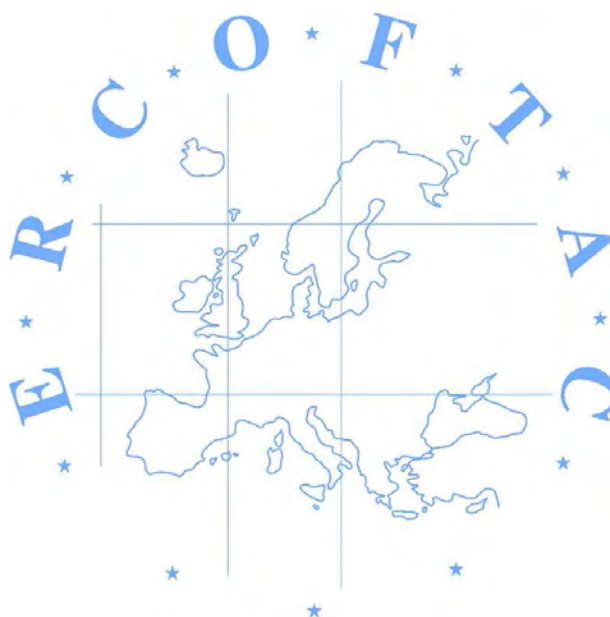
Without fibre suspension flows, the paper upon which you read this text (or might consider printing it on!) would not exist. Fibre suspension flows are vital in papermaking, one of the major material processes in the world. In fact, the annual paper production is three times (measured by mass) the production of plastics and composites! However, although the Special Interest Group 43 (SIG43) "Fibre suspension flows" has its roots in the needs of the pulp and paper industries, the activities are of course not limited to that single application of the subject. Furthermore, research of fibre suspension flows has many aspects in common with other ERCOFTAC topics such as dispersed multiphase flows, drag reduction, and turbulence just to mention some of them.

The first initiatives to form SIG43 were taken during the 6th International Conference on Multiphase Flows in Leipzig, July 2007. The group was formally established in May 2008 and has since then had three meet-

ings or workshops in Brussels, Belgium (November 2008), Jyväskylä, Finland (April 2009) and in Stockholm, Sweden (February 2010). This special issue is the first ERCOFTAC Bulletin produced by the group.

The contributions to follow reflect several aspects of fibre suspension flows and SIG 43. We would like to emphasize the strong links between industrial needs and academic research, both when it comes to measurements techniques and simulation methods. Several contributions also demonstrate general issues, and the inherent complexity, of flows with non-spherical particles. The field poses a wide variety of challenges, ranging from understanding the fundamental physics of particle motion to how to do appropriate simulations of industrial flows and obtain the experimental data necessary to verify them.

This bulletin gives an overview of some of the activities presently going on in Europe. We hope you will enjoy the reading!



DNS OF NON-SPHERICAL PARTICLES IN TURBULENT FLOWS

Helge I. Andersson,¹ Lihao Zhao¹

¹Department of Energy and Process Engineering,

Norwegian University of Science and Technology (NTNU), Trondheim, Norway

helge.i.andersson@ntnu.no, lihao.zhao@ntnu.no

Abstract

Dilute suspensions of elongated solid particles in turbulent gas or liquid flow offer problems of even greater complexity than mono-phase turbulence. Such particulate flows are of immense practical concern both in nature and technology, e.g. airborne solid particles (aerosols), tiny carbon nanotubes, micro-organisms (e.g. phytoplankton), sediment-laden flows, and last but not least suspensions of cellulose fibers. The dynamics of non-spherical particles are equally important and yet by far more complex than the dynamics of spheres suspended in fluid turbulence. This paper aims to give an overview of on-going research on fiber suspension flows at NTNU in Trondheim. The aim of our investigations is to better understand how elongated particles are dispersed in a turbulent shear flow and how the turbulence is modulated by the presence of the non-spherical particles. To enable an in-depth exploration of particle-laden turbulent flows, Eulerian direct numerical simulations in conjunction with two-way coupled Lagrangian particle dynamics are performed.

Introduction

Dilute suspensions of solid particles in turbulent gas or liquid flow offer problems of greater complexity than mono-phase turbulence, but are nevertheless of immense practical concern both in nature and technology. The vast majority of investigations are focused on spherical particles. Non-spherical particles are, however, equally important and their dynamical behaviour is by far more complex than the dynamics of spheres. The transport of fibrous particles is a notable example, which is of particular concern for the present thematic issue of the ERCOFTAC Bulletin. Suspensions of cellulose fibers in water represent a major challenge in the pulp and paper industry. Let us nevertheless also mention some other application areas in which the dynamics of tiny non-spherical particles immersed in a carrier fluid are of crucial importance.

The field of aerosol science and technology has grown in response to the need to understand and control natural and manmade aerosols. The term aerosol technically refers to airborne solid particles (also called dust or particulate matter) or liquid droplets and implies that the matter “floating” in air is a suspension (a mixture in which solid or liquid or combined solid-liquid particles are suspended in air). Similarly, dispersions refer to suspensions of tiny (sub-microscopic) particles in a liquid. Aerosols occur naturally, e.g. from forest fires and volcano eruptions like the recent one from Eyjafjallajökull at Iceland, and from human activities, notably by burning of fossil fuels. Relatively large particles are filtrated

in the nose and throat of human beings and do therefore not cause any health problems. Smaller particles, typically smaller than 10 micrometers, are inhaled without being filtrated and give rise to a multitude of different diseases. Particulate pollution is estimated to cause 20 000 – 50 000 deaths per year only in the United States (Mokdad et al. [1]).

Carbon nanotubes (CNTs) have received immense attention in recent years due to their novel and useful properties. Notable examples of their potential use are found both in the car and electronic industries. The cylinder-shaped CNT typically has a diameter of a few nm and a length of say 10 μ m. CNTs are so small that they can be inhaled deep into the lungs. Since the early 1960s the dangers of asbestos fibers have been in focus. Recently, potential hazards associated also with the foreseen extensive use of CNTs have been addressed for instance by Donaldson et al. [2].

The dynamical behaviour of micro-organisms in the sea can be considered as a dilute particle suspension. Photosynthesizing microscopic organisms inhabit the euphotic (i.e. sunlit) upper layer of the ocean. The phytoplankton is an essential ingredient in aquatic ecosystems and their motions and orientations in the turbulent environment affect for instance their feeding abilities (Mann et al. [3]) and in turn the potential for phytoplankton blooming (Ghosal & Mandre [4]). Particles dispersed in a carrier fluid are also encountered in a great variety of engineering processes, for instance in sediment-laden channel flow, pulverised combustion, sprays etc.

Turbulent dispersion and turbulence modulation are generally significant mechanisms in particulate two-phase flows, see e.g. Parthasarathy [5]. The motion of the individual spherical particles is strongly affected by the turbulent fluid motion and the idealized picture of uniformly dispersed particles is rarely observed in reality. In practice, solid particles have a tendency to accumulate close to a solid surface, see e.g. Eaton & Fessler [6] and the recent review by Balachandar & Eaton ([7]).

Computational modeling of suspensions of non-spherical particles

Solid particles suspended in fluid flow constitute a many-body dynamical problem intricately coupled with a continuum flow problem. The behaviour of elongated (i.e. non-spherical) particles has recently been studied by Yin et al. [8], Manhart [9], Paschkewitz et al. [10-11], Hölzer & Sommerfeld [12] and Gillissen et al. [13-15] with some different statistical representations of the particles.

We follow an alternative approach in which the both the fluid flow and the particle motion are based on so-called ‘first principles’, i.e. the fundamental laws of mechanics. This means that the flow field is obtained di-

rectly from the Navier-Stokes equations while the particle dynamics is governed by equations of translational and rotational motion for each and every particle. This is known as the Euler-Lagrangian approach and has already been used to study motions of elongated fiber-like particles in laminar flows by for instance Högberg et al. [16] and Lundell & Carlsson [17] and in turbulent flows by Zhang et al. [18], Mortensen et al. [19-20] and Marchioli et al. [21]. The last-mentioned investigations follow the same basic modeling principles as in the pioneering study by Zhang et al. [18] and our current work aims to extend this approach in some different directions with the view to improve the physical realism of the computational modelling.

Present methodology

Whereas the turbulent fluid motion can be faithfully reproduced by accurately integrating the full Navier-Stokes equations in space and time, i.e. by an Eulerian representation, the motion of each solid particle is governed by its own equations of motion, i.e. by a Lagrangian representation. It is noteworthy that the Eulerian fluid equations are solved in a fixed frame of reference $[x, y, z]$ whereas the Lagrangian particle equations of motion are solved in a non-inertial coordinate system $[x', y', z']$ attached to the individual particles.

A. Particle shape

Our primary objective is to study the motion of non-spherical particles in turbulent flows. As a representative model of non-spherical particles we consider *ellipsoidal* particles. Each particle is then characterized by three independent length scales $a, b,$ and c as:

$$\frac{x'^2}{a^2} + \frac{y'^2}{b^2} + \frac{z'^2}{c^2} = 1 \quad (1)$$

For simplicity we assume that $a = b,$ i.e. an ellipsoid of revolution about the polar z' -axis, and the ellipsoid becomes a spheroid. Each spheroidal particle is thus characterized by two independent geometrical parameters, namely its size taken as the equatorial radius a and its aspect ratio $c/a.$ Such spheroids can be either *oblate* if $c < a$ or *prolate* when $c > a.$ When $c/a \gg 1$ the spheroids mimic elongated particles and when $c/a \ll 1$ the spheroids resemble disks. The special case $c/a = 1$ corresponds to the more trivial but immensely important case of spherical particles. For such isotropic particles, the particle orientation does not matter. For this reason the spinning of spherical particles embedded in a turbulent flow field has just recently been considered by Mortensen et al. [19]. Our focus of attention is on prolate spheroids which are considered as appropriate models of fiber-like particles and carbon nanotubes (CNTs); see Figure (1)

B. Eulerian approach to wall-bounded turbulent shear flows

We are concerned primarily about the particle behaviour in wall-bounded turbulent flows, notably in pipes and channels. Since the principle features of wall-turbulence are the same in plane channels and pipes with circular cross-section, we concentrate for simplicity on plane channels flows. The flow in a plane smooth-walled channel is characterized only by the Reynolds number. In order to allow for direct numerical simulations (DNSs) the Reynolds number should be moderately low to enable

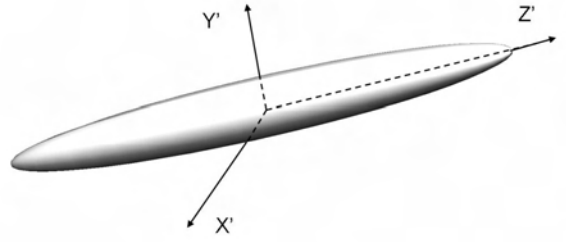


Figure 1: A schematic of a prolate spheroid with an aspect ratio of about to 5. The major or polar axis is aligned with the z' -direction in the particle coordinate system which has its origin in the center of the spheroidal particle.

fully resolved DNS and yet sufficiently high to assure that the flow is in the fully turbulent regime. For pressure-driven pipe and channel flow, a bulk Reynolds number of about 5000 is appropriate and almost all computational studies of dilute particle suspensions have been performed at Reynolds number close to this.

The complete time-dependent Navier-Stokes equations of motion:

$$\nabla \cdot \vec{u} = 0; \quad \rho \left[\frac{\partial \vec{u}}{\partial t} + (\vec{u} \cdot \nabla) \vec{u} \right] = -\nabla p + \mu \nabla^2 \vec{u} + \vec{F}_P \quad (2)$$

are solved in three-dimensional space on an extremely fine grid. Here, \vec{u} and p are the instantaneous fluid velocity vector and pressure, respectively, whereas \vec{F}_P denotes the force per unit volume from the particles. ρ and μ are the density and the dynamic viscosity of the incompressible Newtonian carrier fluid. The computational Cartesian mesh, on which the above PDEs are discretised, should be sufficiently fine so that all scales of the turbulent motion are resolved. The grid spacing should therefore be of the order of the Kolmogorov scale. Implicit in this Eulerian approach is that the particles are assumed sufficiently small, i.e. smaller than the Kolmogorov length scale, and the suspension is sufficiently dilute so that the particles do not displace fluid.

The computer simulations will be performed with the tailor-made DNS code developed at TU Delft and used for instance by Gillissen et al. ([13-15] and Mortensen et al. [19-20,22]). This is a pseudo-spectral flow solver for the incompressible Navier-Stokes equations. The spatial derivatives are computed with a Fourier-basis for the homogeneous directions and second-order accurate central-differences in the wall-normal direction. The explicit time integration is achieved by a second-order Adams-Bashforth scheme. Mass conservation is assured by a standard projection method and the resulting Poisson equation is transferred to Fourier space in the homogeneous directions and a tri-diagonal solver is used for the resulting band matrices.

C. Lagrangian particle dynamics

The motion of the ellipsoidal particles is governed by separate equations for the translational and rotational motion of each individual particle:

$$m \frac{d\vec{v}}{dt} = \vec{f} \quad (3)$$

$$I'_{xx} \frac{d\omega'_x}{dt} - \omega'_y \omega'_z (I'_{yy} - I'_{zz}) = N'_x \quad (4)$$

Here, \vec{v} is the velocity vector and $\vec{\omega}$ is the angular velocity vector of a particle with mass m and principle moments of inertia I'_{xx} etc. The first of these equations is nothing but Newton's 2nd law of translational motion, whereas the latter Euler equation governs the rotational particle motion about the x' -axis and similar equations apply in the two other coordinate directions.

The former includes the force \vec{f} and the latter the torque \vec{N}' exerted by the fluid on the particles. The forces and torques on the particles involve the velocity and the spin of the particles relative to the fluid. The particles are smaller than the Kolmogorov length scale of the turbulence, the particle Reynolds number is below unity and the surrounding flow field can then be considered as creeping. With these assumptions, i.e. the flow in the immediate vicinity of a particle is Stokesian, we adopt the following expressions for the force:

$$\vec{f} = \mu K (\vec{u}' - \vec{v}') \quad (5)$$

Here, K is the resistance tensor K' expressed in the fixed laboratory frame. The torque from the surrounding fluid onto an ellipsoidal particle was derived by Jeffery [23] based on the assumption of Stokes flow. In the special case of spherical particles the resistance tensor simplifies to a scalar constant. The particle relaxation time τ_p can then be derived by introduction of the Stokes force Eq. (5) in Newton's equation of translational motion Eq. (3). For spheroidal particles Zhang et al. [18] derived the more general expression:

$$\tau_p = \frac{2\lambda\rho_p a^2 \ln(\lambda + \sqrt{\lambda^2 - 1})}{9\mu \sqrt{\lambda^2 - 1}} \quad (6)$$

which also were adopted by Mortensen et al. [20,22]. Here, ρ_p is the particle mass density. In the limit as the aspect ratio λ tends to unity, a simpler formula repeatedly used for spherical particles is recovered. It is noteworthy that τ_p is an estimate of how fast a certain particle adjusts to the local fluid motion. As soon as the rotational particle motion also is of interest a separate response time for particle spin should be considered. For spherical particles, we showed that the rotation response time is $0.3\tau_p$ (Mortensen et al. [19]). For the rotational motion of non-spherical particles, however, the definition of a single response time is not feasible since the relaxation inevitably depends on the axis about which the particle rotates.

The transformation between the two coordinate systems involves the three independent Euler angles (ϕ , θ , ψ) which completely specify the orientation of a given particle. In practice, however, we adopted the four Euler parameters (often called quaternions) instead of the Euler angles to connect the fixed reference frame (in which the fluid flow is described) to the particle frame (in which the particle motion is described). To this end equations for the rate-of-change of the Euler parameters are solved.

Thus, in order to obtain the translational and rotational motion of one single non-spherical particle a set of coupled non-linear ordinary differential equations must be integrated numerically in time along with the integration of the Navier-Stokes equations. Eventually, after each and every time step, the new particle position vector is updated according to:

$$\vec{x} = \int \vec{v} dt \quad (7)$$

This Eulerian-Lagrangian approach is essentially the same as that used by Zhang et al. [18] and subsequently

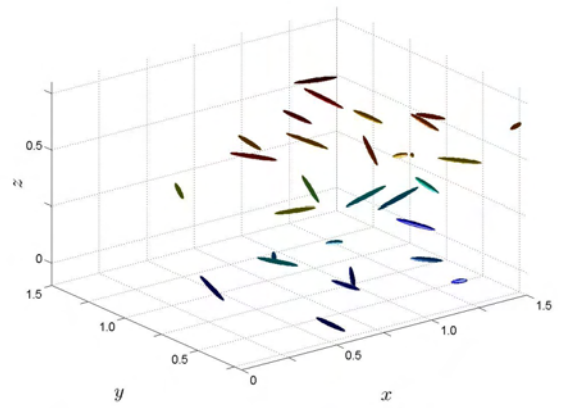


Figure 2: A perspective view of spheroidal particles. The snapshot is taken from a preliminary channel flow simulation with a modest number of particles. This plot shows how differently the prolate spheroids orientate in a turbulent channel flow.

used in channel flow simulations by Mortensen et al. [20,22] and Marchioli et al. [21]. The reader is referred to the article by Mortensen et al. [22] for further details.

The analytical expressions for the forces and torques are based on the assumption of creeping flow, i.e. the so-called particle Reynolds number Re_p based on the relative velocity $\vec{u} - \vec{v}$ should be smaller than unity. For higher Re_p the simple analytical formulas are no longer valid. A wake may occur behind the particle when Re_p is of the order 10. This wake may become unsteady and eventually turbulent. A recent DNS study by El Khoury et al. [24] revealed the complexities of the turbulent wake behind a prolate spheroid with aspect ratio $\lambda = 6 : 1$ and $Re_p = 10\,000$.

D. Coupling between fluid and particles

A *one-way coupled* simulation means that fluid flow does not at all feel the presence of the particles, i.e. \vec{F}_p in Eq. (2) is zero or vanishingly small. This can in many circumstances be a good approximation to reality, for instance if very dilute suspensions are considered. As far as we are aware all earlier computational studies of fiber-like particles using the Eulerian-Lagrangian approach have considered only one-way coupling. Such simulations enable to explore the translational and rotation motion of the elongated particles in a turbulent flow, but the feedback from the particles on the turbulent flow field could not be explored.

Two-way coupling is relatively straightforward for spherical particles, see e.g. Vreman [25] and Balachandar & Eaton [7], but has apparently never been accomplished before for non-spherical particles. For spherical particles, a force from each and every particle has to be included into the 'source' term \vec{F}_p in the Navier-Stokes equations (Eq. (2)). In order to achieve two-way coupling also for non-spherical particles, not only the forces from the particles should be included in the governing flow simulation but also the torques arising from the spinning particles will affect the flow field. Only by means of such two-way coupled simulations, the modulation of the flow field by elongated particles can be explored.

In a one-way coupled simulation of spherical particles, Mortensen et al. [19] showed that tiny spheres rotated with different angular velocities than the fluid rotation in a certain parameter range. We anticipate that the

presence of spinning particles in the carrier fluid also will affect the local rotation of the fluid elements (i.e. the vorticity).

Current developments

Our primary interest is to develop a computational framework for two-way coupled simulations of non-spherical particles like fibers and CNTs. In parallel with these developments we have also paid some attention to Reynolds number effects and for that purpose performed one-way coupled simulations of suspensions of spherical particles at higher Reynolds numbers than those usually considered; see Zhao & Andersson [26].

As a first step towards our ultimate goal, force coupling for spherical particles has been implemented in our computational model. Simulations with only 10^5 particles were almost indistinguishable from results obtained by one-way coupled simulations, i.e. the turbulent flow was almost unaffected by the presence of the spherical particles. With $4 \cdot 10^6$ particles, i.e. greater loading, the turbulent flow field was modulated by the presence of the particles. Of major interest is probably the significant pressure loss reduction achieved. Results from this study have been reported by Zhao et al. [27]. Let us recall that the particle loading has no impact on the fluid flow in one-way coupled simulations. Mortensen et al. [20-22] nevertheless typically used 10^6 particles in order to provide a sufficient basis for evaluation of distribution functions of particle positions, velocities, orientations, and spin. In two-way coupled simulations the particle loading becomes an essential parameter.

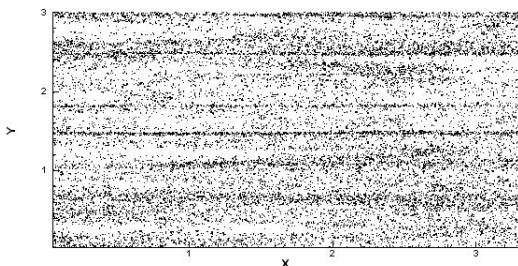


Figure 3: Particle distributions in a plane parallel with the walls. This instantaneous view is taken from the two-way coupled simulation of spherical particles with $\tau_p^+ = 30$ reported by Zhao et al. [27]. The tendency of the spheres to concentrate in certain streamwise bands seems to be more pronounced than in one-way coupled simulations.

In order to perform two-way coupled simulations of suspensions of non-spherical particles, not only a force-coupling is required but also the issue of torque-coupling becomes important. While the force-coupling between the fluid and a particle relies on Newton's 3rd law, an analogous law holds for the torques, i.e. the torque from a given particle onto the fluid is the same (but oppositely directed) of the torque \vec{N}' from the fluid on that particle in Eq. (4). It is not obvious how such a torque should be introduced into the Navier-Stokes equations (Eq. (2)). Inspiration as to how this can be accomplished is currently sought in the micro-continuum fluid mechanics literature, notably within the framework for modelling micropolar fluids pioneered by Eringen [28]. The development, implementation, testing and exploration of the torque coupling constitute central ingredients in our current research.

Acknowledgements

The early stages of this work were financially supported by The Research Council of Norway (NFR) through the PETROMAX programme. The work is currently funded by NFR (project no 191210/V30) and by A/S Norske Shell (contract no 4610020178/C08156). Computing time on the 'Stallo' compute cluster HP BL 460c in Tromsøis granted by NFR (Programme for Supercomputing). The collaboration with Prof. B.J. Boersma and Dr. J.J.J. Gillissen (TU Delft) and Dr. M. Barri (NTNU) is greatly appreciated.

References

- [1] A.H. Mokdad, J.S. Marks, D.F. Stroup and J.L. Gerberding "Actual causes of death in the United States, 2000", *Journal of the American Medical Association*, Vol. 291, 2004, pp. 1238-1245.
- [2] K. Donaldson, R. Aitken, L. Tran, V. Stone, R. Duffin, G. Forrest & A. Alexander (2006) "Carbon nanotubes: a review of their properties in relation to pulmonary toxicology and workplace safety", *Toxicological Sciences*, Vol. 92, 2006, 5-22.
- [3] J. Mann, S. Ott, H.L. Pecseli & J. Trulsen "Laboratory studies of predator-prey encounters in turbulent environments: effects of changes in orientation and field of view", *Journal of Plankton Research*, Vol. 28, 2006, pp. 509-522.
- [4] S. Ghosal & S. Mandre "A simple model illustrating the role of turbulence on phytoplankton blooms", *Journal of Mathematical Biology*, Vol. 46, 2003, pp. 333-346.
- [5] R.N. Parthasarathy "An overview of experimental observations of turbulent dispersion and turbulent modulation in dilute multiphase flows", 44th AIAA Aerospace Sciences Meeting, 2006, AIAA Paper 2006-1520.
- [6] J.K. Eaton & J.R. Fessler "Preferential concentration of particles by turbulence", *International Journal of Multiphase Flow*, Vol. 20 (Suppl), 1994, 169-209.
- [7] S. Balachandar & J.K. Eaton "Turbulent dispersed multiphase flow," *Annual Review of Fluid Mechanics*, Vol. 42, 2010, 111-133.
- [8] C. Yin, L. Rosendahl, S.K. Kær & H. Sørensen "Modelling the motion of cylindrical particles in a nonuniform flow", *Chemical Engineering Science*, Vol. 58, 2003, pp. 3489-3498.
- [9] M. Manhart "Rheology of suspensions of rigid-rod like particles in turbulent channel flow", *Journal of Non-Newtonian Fluid Mechanics*, Vol. 112, 2003, pp. 269-293.
- [10] J.S. Paschkewitz, Y. Dubief, C.D. Dimitropoulos, E.S.G. Shaqfeh & P. Moin "Numerical simulation of turbulent drag reduction using rigid fibres", *Journal of Fluid Mechanics*, Vol. 518, 2004, pp. 281-317.
- [11] J.S. Paschkewitz, C.D. Dimitropoulos, Y.X. Hou, V.S.R. Somandepalli, M.G. Mungal, E.S.G. Shaqfeh & P. Moin "An experimental and numerical investigation of drag reduction in a turbulent boundary layer using a rigid rodlike polymer", *Physics of Fluids*, Vol. 17, 2005, 085101.
- [12] A. Hölzer & M. Sommerfeld "Lattice Boltzmann simulations to determine forces acting on non-spherical particles", *Proc. IUTAM Symposium on Computational Approaches to Multiphase Flow*, Springer Verlag, 2006, pp. 99-108.
- [13] J.J.J. Gillissen, B.J. Boersma, P.H. Mortensen & H.I. Andersson "On the performance of the moment approximation for the numerical computation of fibre stress in turbulent channel flow", *Physics of Fluids*, Vol. 19, 2007, 035102.
- [14] J.J.J. Gillissen, B.J. Boersma, P.H. Mortensen & H.I. Andersson "The stress generated by non-Brownian fibres in turbulent channel flow simulations", *Physics of Fluids*, Vol. 19, 2007, 115107.
- [15] J.J.J. Gillissen, B.J. Boersma, P.H. Mortensen & H.I. Andersson "Fibre-induced drag reduction", *Journal of Fluid Mechanics*, Vol. 602, 2008, 209-218.
- [16] S.M. Högberg, H.O. Åkerstedt, T.S. Lundström & J.B. Freund "Numerical model for fiber transport in the respiratory airways", *Proc. 19th International Symposium on Transport Phenomena, Reykjavik (Iceland) 17 - 21 August 2008*.
- [17] Lundell & A. Carlsson "Heavy ellipsoids in creeping shear flow: transitions of the particle rotation rate and orbit shape", *Physical Review A*, Vol. 81, 2010, 016323.
- [18] H. Zhang, G. Ahmadi, F.G. Fan & J.B. McLaughlin "Ellipsoidal particle transport and deposition in turbulent channel flows", *International Journal of Multiphase Flow*, Vol. 27, 2001, 971-1009.
- [19] P.H. Mortensen, H.I. Andersson, J.J.J. Gillissen & B.J. Boersma "Particle spin in a turbulent shear flow", *Physics of Fluids*, Vol. 19, 2007, 078109.

- [20] P.H. Mortensen, H.I. Andersson, J.J.J. Gillissen & B.J. Boersma “On the orientation of ellipsoidal particles in a turbulent channel flow”, *International Journal of Multiphase Flow*, 34, 2008, 678-683.
- [21] C. Marchioli, M. Fantoni & A. Soldati “Orientation, distribution, and deposition of elongated, inertial fibers in turbulent channel flow”, *Physics of Fluids*, Vol. 22, 2010, 033301.
- [22] P.H. Mortensen, H.I. Andersson, J.J.J. Gillissen & B.J. Boersma “Dynamics of prolate ellipsoidal particles in a turbulent channel flow” *Physics of Fluids*, Vol. 20, 2008, 093303.
- [23] G.B. Jeffery “The motion of ellipsoidal particles immersed in a viscous fluid”, *Proceedings of the Royal Society of London A*, Vol. 102, 1922, 161-178.
- [24] G.K. El Khoury, H.I. Andersson & B. Pettersen “Crossflow past a prolate spheroid at Reynolds number 10000”, *Journal of Fluid Mechanics*; 2010, in print.
- [25] A. Vreman “Turbulence characteristics of particle-laden pipe flow”, *Journal of Fluid Mechanics*, Vol. 584, 2007, pp. 235-279.
- [26] L.H. Zhao & H.I. Andersson “Statistics of particle suspensions in turbulent channel flow”, 8th Asian Computational Fluid Dynamics Conference, Hong Kong, 10-14 January, 2010.
- [27] L.H. Zhao, J.J.J. Gillissen & H.I. Andersson “Turbulence modulation and drag reduction by spherical particles”, *Physics of Fluids*; Vol. 22, 2010, in print.
- [28] A.C. Eringen “Theory of micropolar fluid”, *Journal of Mathematics and Mechanics*, Vol. 16, 1966, pp. 1-18.

ELECTRICAL RESISTANCE TOMOGRAPHY TECHNIQUE IN PULP AND PAPER INDUSTRY

Lasse Heikkinen,¹ Jari Kourunen,¹ Petteri Paananen,² Kari Peltonen,³ Jari Käyhkö,² Marko Vauhkonen¹

¹Department of Physics and Mathematics, University of Eastern Finland, P.O.Box 1627, FIN-70211, Kuopio, Finland

²FiberLaboratory, Lappeenranta University of Technology, Savonlinna, Finland.

³Andritz Oy, Kotka, Finland.

Abstract

Electrical resistance tomography (ERT) is a tomographic imaging modality in which the internal conductivity distribution of the target volume is estimated based on the electrical measurements made on the object's surface. ERT can be used in pulp and paper industry for on-line monitoring of e.g. homogeneity of pulp flow and mixing efficiency of pumps and mixers. In this paper we show recent results of using ERT in chemical mixing study and in evaluation of an MC mixer.

Introduction

Electrical resistance tomography (ERT) is a tomographic imaging modality in which the internal conductivity distribution of the target volume is estimated based on the known injected electric currents and voltages on the surface of the object. On the basis of the conductivity distribution, the internal structure or state of the object could be evaluated. ERT imaging technique can be utilized in many different applications in medicine and industry (Vauhkonen et al. [10]). It is especially suitable for process tomographic applications in pulp and paper industry since ERT can produce reconstructions with the speed fast enough for imaging pulp flow (Heikkinen et al. [4] and Kourunen et al. [7]). Modern measurement systems and image reconstruction algorithms can produce up to 40 three-dimensional images per second (Kourunen et al. [8]).

In this paper, we consider utilizing three-dimensional ERT imaging in pulp and paper industry. We consider two different application cases, LC (low consistency) pulp flow imaging and evaluation of an MC (medium consistency) mixer. In all the studies we have used an imaging system KIT4 developed at the University of Eastern Finland, Kuopio, Finland (Kourunen et al. [8]).

Application of ERT to LC pulp flow measurements

There are many applications in pulp and paper industry in which LC flows exist. Good example is a short circulation of paper making process. There is a need for a technique to measure pulp consistency, air content and mixing quality. Electrical resistance tomography can offer the opportunity to monitor these variables.

In this case study, the monitoring of mixing of retention chemical to the LC pulp flow was considered. The measurements were carried in a laboratory flow loop made of transparent plastic. The part of the loop is shown in Figure (1). The inner diameter of the pipe is 100mm. 80 stainless steel electrodes were attached on

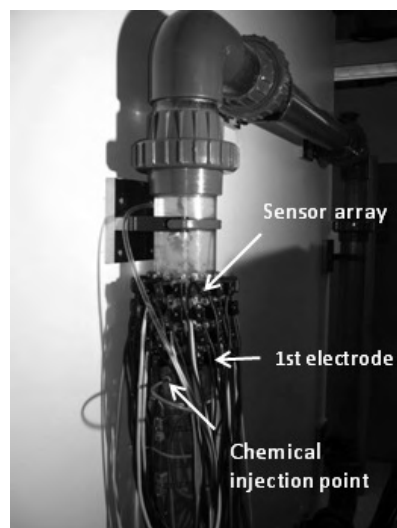


Figure 1: Measurement setup for LC pulp flow study. The direction of the flow was upwards.

the surface of the pipe. They were arranged in four different layers, sixteen electrodes per layer. The length of the ERT sensor was 130 mm. 16 current injection channels and 64 voltage measurement channels were used.

The consistency of the pulp was 1.69% and it was estimated using loss of drying method. An ultrasound sensor was used to measure the flow velocity which was 0.36 m/s. One 30 ml burst of retention chemical was injected to the flow through a small valve which was located just below the ERT sensor.

Three-dimensional conductivity distribution was estimated using the approach presented e.g. in (Heikkinen et al [4]). The reconstruction method is based on statistical inversion theory, for more information see (Kaipio and Somersalo, [5]). The conductivity distribution during the chemical injection is shown in Figure (2). More conductive retention chemical can be seen on the left side of the pipe just above the injection point. It can also be seen that the mixing of the chemical is not complete. On the basis of the conductivity distribution, the mixing efficiency can be quantified by calculating a mixing index (Bennington et al [1]). Using different consistency levels it was also found that the chemical mixing can be monitored within the whole LC range.

Application of ERT to the evaluation of an MC mixer

Mixing of chemicals in pulp bleaching is an important process in the paper production. In bleaching process, the color of the pulp is removed so that the pulp bright-

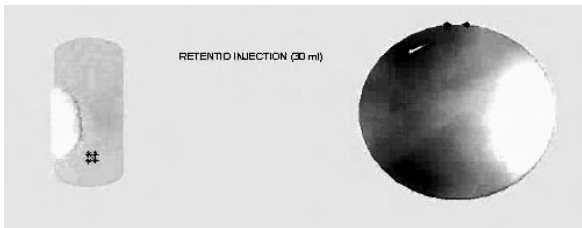


Figure 2: The estimated conductivity distribution in the case of the injection of the retention chemical. Right: Three dimensional distribution as an iso-surface. The dots denote the place of the first measurement electrode, see Figure 1. Left: Two dimensional cross-section of the conductivity distribution. Two dots on the top denote the place of the first measurement electrode.

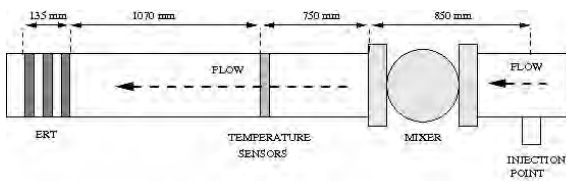


Figure 3: Measurement setup for MC-mixer study. The diameter of the pipe was 300 mm.

ness increases. Chemicals are mixed in to the pulp using e.g. an MC-mixer. Efficient mixing is very important factor in the design of bleaching mixer and economic production of paper (Bennington et al. [1-2]). Therefore, characterization of mixing efficiency of the mixer is essential. Several methods have been developed to evaluate the performance of the mixers (Rewatkar et al. [9], Kamal and Bennington [6], Bennington et al. [1-2])

Temperature profiling is a non-invasive method which can be used to evaluate the quality of mixing (Rewatkar et al. [9]). In this method, several temperature sensors are attached on the periphery of the process pipe. Based on the measured temperature profiles, the mixing index and/or efficiency of the mixer can be estimated. The disadvantage of this method is that the information is acquired only from the boundary of the pipe and therefore the mixing inside the process pipe is not exactly known. Another problem is that the time response of the temperature sensors is not fast enough, being usually around 1 s. This can be a problem especially in high speed flows.

The objective of this work was to evaluate suitability of ERT for MC-pump efficiency measurements. The measurement setup is shown in Figure (3). On the periphery of the pipe, eight temperature sensors were attached, at the distance of 750 mm from the mixer. The ERT sensor was placed at the distance of 1820 mm from the mixer. The sensor consisted of 48 electrodes on three different layers.

The consistency of the pulp was 10% and the mass flow was 150 l/s, the velocity of the pulp suspension in the pipe was in a range $>2,0$ m/s. Cold water was used as a tracer and it was injected to the main flow from the injection point, see Figure 3. In the beginning of the experiment only the main flow was on. At about 6 s after the beginning of the experiment the injection of water was switched on. At about 22 s after the beginning, the mixer was switched on and at about 38 s it was switched off.

The results are shown in Figure (4) and Figure (5). In Figure (4), both the temperature profiles from 4 sensors

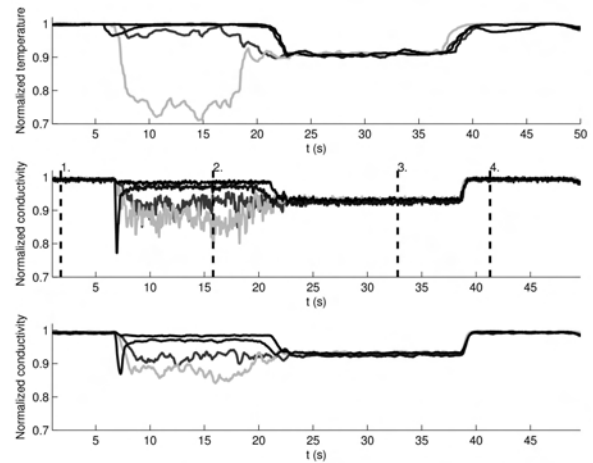


Figure 4: Top: The normalized temperature profiles of the four sensors as a function of time. Middle: The normalized conductivity values of areas on the proximity of the four temperature sensors. The vertical black lines denote times at which the reconstructions shown in Figure 5 are computed. Bottom: The filtered (windowed average) data of the conductivity.

and the estimated conductivity values on the proximity of 4 temperature sensors as a function of time is shown. As it can be seen, both methods are able to detect the cold water injection. Moreover, the effect of the mixer can also be seen in the temperature and conductivity data.

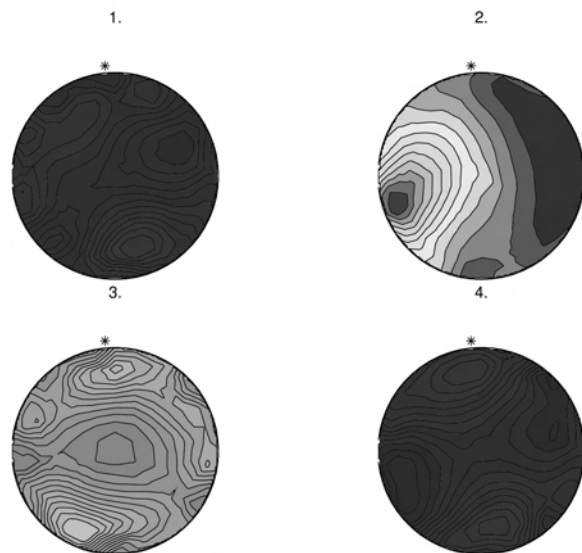


Figure 5: The estimated conductivity distributions at the times shown in Figure (4). Upper left: Only the main flow on. Upper right: The main flow and water injection on. Lower left: The main flow, water injection and mixer on. Lower right: Only the main flow on.

The advantage of the ERT over the temperature measurements can be seen in Figure (5). From the cross-sectional images it can be seen that the mixing is not homogeneous when the mixer is off (upper right image), whereas when the mixer is on, the injected water is homogeneously distributed in the main flow (lower left image).

Conclusion

In this paper we have demonstrated the possibility of using ERT in pulp and paper industry for imaging LC pulp flow and efficiency of an MC mixer. The results show that ERT produces new information compared to the traditional point measurements techniques, such as temperature measurements. Being an on-line measurement technique, ERT can be used in real industrial environments for real time process monitoring and control.

References

- [1] Bennington C.P.J. (2004): Mixing in the pulp and paper industry, In: Paul E.L., Atiemo-Obeng V.A., Kresta S.M. (ed.), Handbook of Industrial Mixing, John Wiley & Sons, Inc. New Jersey, pp. 1187-1246.
- [2] Bennington C.P.J., Peters C.M. and MacLaren R. (1997): Characterization of mixing quality in laboratory pulp mixers, *J. Pulp Paper Sci.* 23(9), 459.
- [3] Bennington C.P.J., Yang H.T. and Pageau G. L. (2001): Mill assessment of mixing quality using laboratory bleaching studies, *Pulp paper Can.* 102(11), 23.
- [4] Heikkinen L.M., Kourunen J., Savolainen T., Vauhkonen P.J., Kaipio J.P. and Vauhkonen M. (2006): Real time three-dimensional electrical impedance tomography applied to multiphase flow imaging, *Measurement Science and Technology*, 17, 2083-2087.
- [5] Kaipio J. and Somersalo E. (2004): Statistical and computational inverse problems (Springer, New York).
- [6] Kamal N.R. and Bennington C.P.J. (2000): An On-line, In-situ, mixing assessment technique for pulp fibre suspensions, *J. Pulp Paper Sci.* 26(6), 214.
- [7] Kourunen J., Käyhkö R., Matula J., Käyhkö J., Vauhkonen M. and Heikkinen L.M. (2008): Imaging of mixing of two miscible liquids using electrical impedance tomography and linear impedance sensor, *Flow Measurement and Instrumentation*, 19, 391-396.
- [8] Kourunen J., Savolainen T., Lehtikoinen A., Vauhkonen M. and Heikkinen L.M. (2009): Suitability of a PXI platform for an electrical impedance tomography system, *Measurement Science and Technology*, 20 015503 (11pp) doi:10.1088/0957-0233/20/1/015503.
- [9] Rewatkar, V.B., Kerekes R.J. and Bennington C.P.J. (2002): Use of temperature profiling to measure mixing quality in pulp bleaching operations, *Pulp Paper Can.* 103(7), 21.
- [10] Vauhkonen P.J., Vauhkonen M., Savolainen T. and Kaipio J.P. (1999): Three-dimensional electrical impedance tomography based on the complete electrode model, *IEEE Trans Biomed Eng.* 46, 1150 - 116.

ON THE FLOW BEHAVIOUR OF WOOD FIBRE SUSPENSIONS

Ari Jäsberg¹

¹Department of Physics, University of Jyväskylä, Finland
VTT Technical Research Centre of Finland
ari.u.jasberg@jyu.fi

Background

We consider here the behaviour of wood fibre suspension with fibre concentration above that of sedimentation in a pressure driven flow in a straight pipe with smooth walls. According to Duffy, the flow behaviour of wood fibre suspensions can be roughly divided in two main regimes: the plug-flow regime that occurs at low flow rates and the drag reduction regime that occurs at high flow rates [1, 2]. Within the plug-flow regime the fibre phase moves as a continuous fibre network with solid like properties and with no shearing motion. In this regime, the loss is high compared to that of the carrier fluid (usually water) at the same flow rate. Furthermore, the dependence on flow rate of loss can be quite complicated. In some cases the loss may decrease with increasing flow rate. In the drag reduction regime, the fibre network is partly or entirely broken into flocs that undergo turbulent and shearing motion. Characteristic to this region is that the frictional loss may be below that of a pure carrier fluid. These qualitatively different main regimes can be further divided into several sub-regimes [1, 2].

Although this flow behaviour is relatively well known, this general knowledge is not sufficient for providing us with loss correlations that are similar to those of Newtonian fluids. There have been several attempts to model measured loss behaviour [3, 4, 5]. The practical design equations used in the industry are based on experimental correlations utilizing a large amount of data but relatively vague theoretical reasoning, see *e.g.* [6]. The design principles are thus quite conservative and omit many fine details of the flow behaviour.

The purpose of the research outlined below is to utilize relatively new experimental methods in order to gain more detailed understanding on the flow behaviour of wood fibre suspensions, and especially on the relevant physical phenomena inducing such behaviour. In addition, the experimental results have been used in modeling the observed loss behaviour. Further details on the experimental methods and modeling work can be found in Ref. [7].

Experimental work

The flow experiments have been carried out with a laboratory-scale acrylic flow loop with pipe diameter 40 mm at University of Jyväskylä, as well as with pipe diameters 100 mm and 200 mm at VTT Technical Research Centre of Finland. The flow rate has been measured using a magnetic flow meter and the flow loops have been equipped with a differential pressure transducers for standard loss measurement. So far, simple suspensions consisting of water and chemically released long (pine) or short (birch) fibres have been studied.

In a widely adopted view the plug-flow regime where the loss saturates or decreases with increasing flow rate is caused by a sub-millimeter thick layer of pure water that

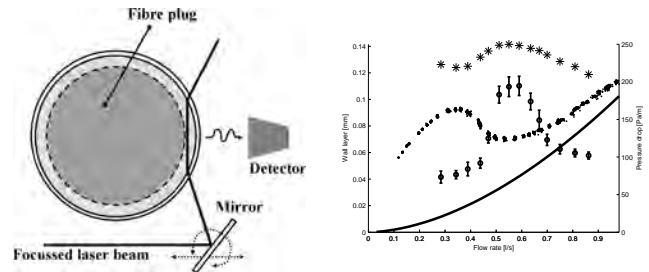


Figure 1: Left) The principle of laser-optical measurement of the lubrication layer. Right) Measured pressure drop (small dots) and wall layer thickness (open circles) versus flow rate for birch suspension at 1.0% in a $D = 40$ mm pipe. Solid line is the pressure drop of water, and stars give the thickness of the viscous sublayer ($y^+ = 5$) for water at each value of loss.

is created between the fibre plug and the pipe wall. However, this view was originally based solely on pure visual observations and on the fact that it can (qualitatively) reproduce the observed loss behaviour, *i.e.* on indirect reasoning. A special laser-optical device has been constructed that can be used to directly measure the thickness of this lubrication layer in a fully developed plug-flow. In the device, a collimated laser beam is guided inside the acrylic flow channel, see Figure (1). The light scattered from fibres traversing the beam is detected by an optical sensor placed just outside the pipe wall, and having a narrow horizontal field of view through the pipe wall into the focal point of the beam.

In Figure (1) (right) are shown the measured values of layer thickness as a function of mean flow velocity for birch fibre suspension. It appears that the regime where the lubrication layer can not be found coincides with the low flow rate domain where the loss increases with flow rate. This domain is naturally identified as the plug-flow regime with direct fibre-wall contact. An observable lubrication layer appears at the flow rate corresponding to the local maximum in the loss curve, and above that flow rate, the measured value of the lubrication layer thickness first grows with flow rate. The flow rate corresponding to the maximum layer thickness falls approximately at the same point where the loss curve again starts to grow. This domain is identified as the plug-flow regime with lubrication layer. The observed decrease of the layer thickness after the maximum is most likely due to incipient turbulence in the fluid phase. This turbulence is not yet strong enough to cause macroscopic breakage of the fibre network, but only to bend and dislodge individual fibres that are loosely bound to the fibre plug surface. This view is supported by the fact that the maximum layer thickness is just below the thickness of the viscous sublayer for water

In the drag reduction regime, flow phenomena are studied by measuring the velocity profiles of fibre phase

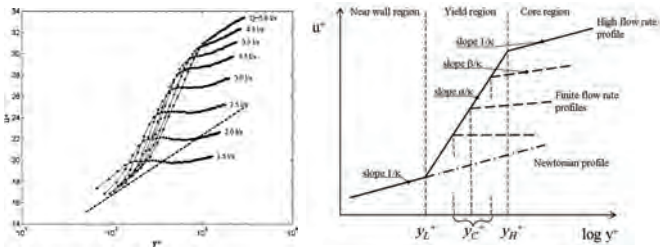


Figure 2: Left) Mean velocity profiles of pine fibre suspension of consistency 1% as a function of distance from the pipe wall expressed with standard non-dimensional wall-layer variables, together with the standard logarithmic Newtonian profile (dashed line). Right) Parameterization of measured velocity profiles.

using pulsed ultrasound Doppler velocimetry (PUDV). Figure 2 (left) shows the measured mean velocity profiles of pine fibre suspension of consistency 1% for flow rate ranging from 1.5 l/s to 5.0 l/s. Due to noise caused by the wall-fluid interface, the velocity measurement by the PUDV method is not accurate below 1 mm from the wall, and those results are excluded from the profiles shown. Also shown in the figure is the standard logarithmic Newtonian profile

$$u^+ = \frac{1}{\kappa} \ln(y^+) + B. \quad (1)$$

A remarkable feature of the experimental profiles shown in Figure 2 is that there seems to exist a unique (approximate) envelope curve (the solid line in the right figure) that corresponds to a limiting velocity profile shape as the flow rate approaches infinity. That envelope curve consists of a logarithmic near wall region where the profile coincides with that of Newtonian flow, a yield region where velocity gradient is higher than that of Newtonian flow, and a core region where the profile again is of the form given by Eq. (1) but with a value of constant B above that of Newtonian flows. The drag reduction regime is a direct consequence of the increased velocity (gradient) in the yield region, thus within the present reasoning that regime could more accurately be described as the 'regime of flow enhancement'.

Modelling of loss

The modelling work utilizes modeled velocity profiles in the plug-flow regime and the experimental velocity profiles in the drag reduction regime. The flow rate corresponding to a given friction velocity/wall stress (that yields the loss) is found simply by integrating the velocity profile over the pipe cross section. In the plug-flow regime, the velocity profiles are governed by a two-phase model that conserves mass and momentum for both phases, fibres and water, separately. The model includes transfer of momentum due to interaction between the phases. In the direction of the mean flow the interaction is described by Darcy's drag force that is linear in the drift velocity between the phases. In the transverse direction, the interaction is described as a hydrodynamic lift force acting on the fibres. In the model, the lift force is responsible for existence of the lubrication layer between the fibre plug and the pipe wall. The model contains a set of physical parameters which are determined by a least-squares fit in the experimental loss data.

In the drag reduction regime, the modelling mimics the traditional approach used for Newtonian flows, *i.e.*

it is based on simple parameterization of measured velocity profiles, see Figure 2 (right). The profiles are approximated with a broken line with three segments. The first segment is the Newtonian part in the near-wall region up to depth $y^+ = y_L^+$. The next segment is the yield region with increased slope α/κ up to the depth $y^+ = y_C^+$, after which comes the last segment, the core region. The parameterization takes into account the shift of the transition y_C^+ with flow rate, as well as the increase of the slope β/κ in the core region with increasing flow rate. The profile parameters are determined from a least-squares fit to experimental profile data.

As an example results, in Figure 3) are shown measured values of loss for pine fibre suspension of consistency 1.0% for three pipe diameters together with losses in the plug-flow regime and drag reduction regime as predicted by the corresponding models.

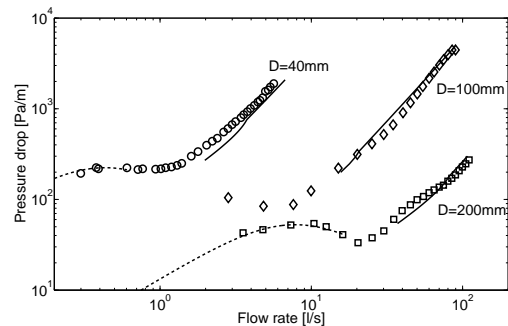


Figure 3: Loss vs. flow rate for pine fibre suspension of consistency 1.0%. The experimental values are shown as open markers, loss in the plug-flow regime predicted by the two-phase model as dashed lines, and loss in the turbulent regime given by the semi-empirical model as solid lines.

References

- [1] G. G. Duffy. The unique behaviour of wood pulp fibre suspensions. In *9th International Conference on Transport and Sedimentation of Solid Particles*, September 1997.
- [2] P. F. W. Lee and G. D. Duffy. An analysis of the drag reducing regime of pulp suspension flow. *Tappi J.*, 59:119–122, 1976.
- [3] W. Brecht and H. heller. A study of pipe friction losses of paper stock suspensions. *Tappi J.*, 33(9), 1950.
- [4] G. D. Duffy. A review and evaluation of design methods for calculating friction loss in stock piping systems. *Tappi J.*, 59(8):124–127, 1976.
- [5] Møller K. and Duffy G. D. An equation for predicting transition-regime pipe friction loss. *Tappi J.*, 61:63–66, 1978.
- [6] TIS0410-14. Generalized method for determining the pipe friction loss of flowing pulp suspensions. Technical report, Tappi J., 1988.
- [7] A. Jäsberg. *Flow behaviour of fibre suspensions in straight pipes: new experimental techniques and multiphase modeling*. PhD thesis, University of Jyväskylä, Jyväskylä, Finland, 2007.

FIBRE SUSPENSION RHEOLOGY RESEARCH AT VTT

Antti Koponen¹

¹VTT Technical Research Centre of Finland.

1 Introduction

The multiphase flows team at VTT has a long background for experimental studies of complicated industrial flows. Our strengths include top-level expertise in pilot-scale research platforms as well as supporting modelling and simulation. In addition to using state of art commercial technology, our team also develops new experimental methods and devices. So far, majority of our applications have involved fiber suspensions found in paper industry, but we have also worked with other rheological substances, such as waste water, mineral slurries, polymer suspensions, and oil. In this paper we give some insight in our work related to fiber suspensions research.

2 Flocculation dynamics of fibers

The uniformity of basis weight (formation) of paper effects on many paper properties such as tensile strength, cockling and print quality. Fibres in a wood pulp suspension have a strong tendency to stick together to form inhomogeneous flocculated networks, flocs, which are known to be an important factor in leading to bad formation. Therefore, the knowledge of fluidisation and reflocculation behaviour of the suspension may provide predictive means to estimate attainable formation with different designs and operational parameters of the paper machine.

At fibre consistencies that exceed the sedimentation consistency, fluidisation and the associated breakage of flocs is attained by inducing turbulent flow. In a headbox, e.g., turbulence is created by wall shear and by sudden expansion steps. By these means, the initial fibre structure is broken into smaller flocs and single fibres with weakly correlated velocities. Due to the presence of fibres, turbulence is effectively damped leading to fast re-growth of floc size in the decaying turbulent field.

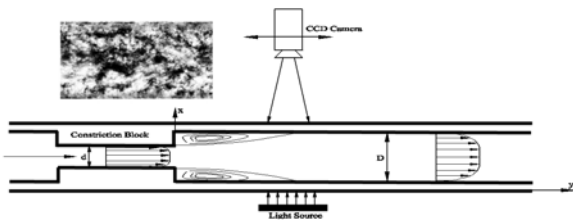


Figure 1: The experimental setup for a sudden expansion. Also shown is one example of an obtained flocculation image.

We have measured the evolution of floc size in various flow conditions using a fast shutter CCD-camera with transmitted light and appropriate image analysis. (In Figure (1), an example of a flocculation image has been shown.) For turbid fluids the characteristic size of the flow has been estimated by using pulsed ultrasound-Doppler anemometry (PUDA) measurements. The turbulent state of the fibrous phase has been characterised

either by capturing velocity fluctuations of fibres with PUDA, or by using successive images for calculating the mobility (“apparent turbulence”) of the pulp suspension.

As an example, we look at the flocculation behaviour of the fiber suspension in an axisymmetric sudden expansion geometry found in real headboxes (see Figure (1)). Figure (2) shows the evolution of 0.5% pine pulp floc size as a function of mean residence time from a step expansion. We have found [1,2], that there are three dynamically different regions in the flow downstream of the step expansion, namely recirculation region, decaying turbulence region and developing pipe flow region. The behavior of the recirculation eddy observed at step heights exceeding the mean fibre length are similar to that found for simple Newtonian fluids. For step heights comparable or less than the mean fibre size, no recirculation eddy is formed. The floc rupture ratio, defined as the ratio of the minimum floc size found at the end of the recirculation region and the floc size upstream of the step has been found to be dependent on the size of the largest scales of the turbulent field, rather than on the overall turbulent intensity. Finally, power law scaling behavior of the floc size with the turbulent intensity has been found in the decaying turbulence region.

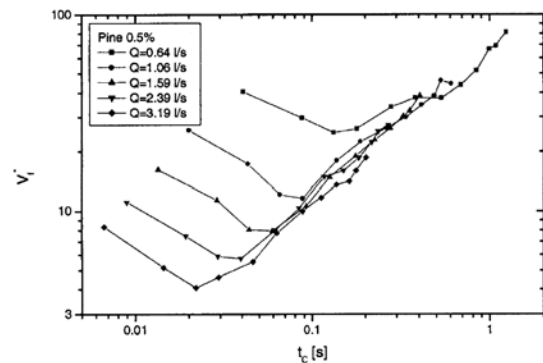


Figure 2: Evolution of floc size as a function of mean residence time from step expansion.

Our flocculation analysis has also been successfully applied e.g. for developing a computational model of floc rupture and re-flocculation in turbulent shear flow [13] and for analysing the performance of laboratory refiners [9].

3 Pressure loss of pulp flow

The central issue in many engineering problems involving fluid flow is estimating frictional losses. For simple Newtonian fluids, loss in a fully developed flow in a straight tube is relatively accurately given by the famous Moody’s diagram, or the related correlation formulas, which summarize the existing (yet incomplete) theoretical understanding on frictional flow in closed channels and a vast amount of carefully measured and analyzed experimental

data. The qualitative flow behaviour of wood fibre suspensions in straight tubes is relatively well known, but it is quantitatively much more complicated than that of pure Newtonian fluids. In some parts of the flow regime, e.g., pressure loss may decrease with increasing flow rate. In this drag reduction regime the frictional loss may even be below that of a pure carrier fluid (see Figure (3)). General knowledge is not sufficient for providing us with accurate loss correlations for these complex fluids. The practical design equations used in the industry are based on experimental correlations utilizing a large amount of data but relatively vague theoretical reasoning. The design principles are thus quite conservative and omit many fine details of the flow behaviour.

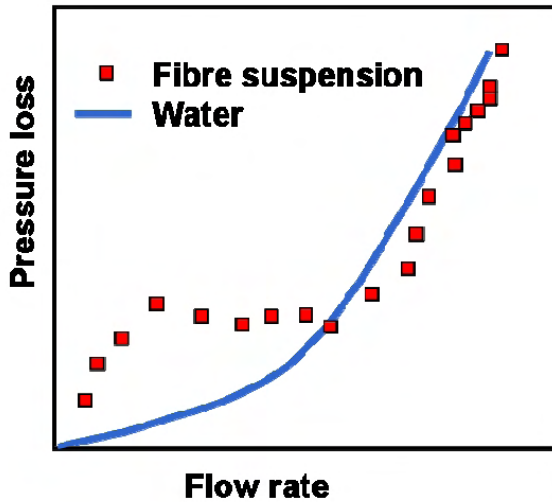


Figure 3: Qualitative behaviour of pressure loss as a function of flow rate for a fully developed flow of fibre suspension in straight smooth tube. The solid line indicates the standard pressure loss behaviour of water.

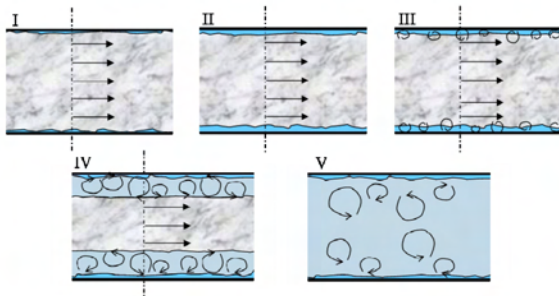


Figure 4: The main flow regimes of fibre suspensions. (I) Plug flow regime with direct fibre-wall contact, (II) plug flow regime with lubrication layer, (III) plug flow regime with incipient (fluid phase) turbulence, (IV) mixed flow regime and (V) fully turbulent flow regime.

The qualitative behaviour of the pulp flow can be explained as follows: If the pressure gradient applied to the tube is below some threshold value that depends on fibre type and concentration the fibre plug does not move at all and the motion of the carrier fluid is described as a flow through porous medium. Above the threshold pressure, also the fibre plug is set into motion. The fibres are first in a direct contact with the wall inducing high shear stress (high loss). As the flow rate is increased, a plug flow behaviour is preserved, but a thin layer of pure water (a 'lubrication' layer) is created next to the wall.

Characteristic to this flow regime is that the wall friction is approximately constant, and may even decrease with increasing flow velocity. As the flow rate increases further, turbulent flow appears near the walls and the fibre plug begins to break from its outer surface. Thus, in this mixed flow regime a turbulent fibre annulus surrounds a rigid fibre plug in the middle of the tube. At some point, frictional loss falls below that of the carrier liquid and drag reduction regime is obtained. As the flow rate is still increased, the solid fibre core gradually vanishes indicating fully turbulent or 'fluidized' flow regime. Here, the loss typically approaches the pure fluid curve asymptotically as the flow rate is increased. The different flow regimes have been summarized in Figure (4).

This quite generally accepted view on the different flow domains was originally based on pressure loss measurements, visual observations of the flow near the tube wall and on velocity profile measurements made at turbulent region using a specific annular purge impact probe. We have investigated this qualitative general flow behaviour in much more detail directly measuring with pulsed ultrasound-Doppler anemometer the fibre velocity field and simultaneously measuring the thickness of the fibre free lubrication layer near the wall with laser optics [3]. The information given by our experimental work has

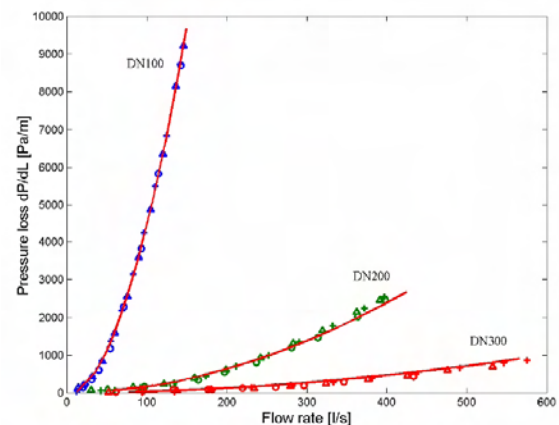


Figure 5: Measured pressure loss as a function of flow rate for 1% commercial fine paper (Δ), LWC (O) and SC (+) pulps. The measurement was done for three different standard steel tubes, DN100 ($\Phi = 110.3\text{mm}$), DN200 ($\Phi = 215.1\text{mm}$) and DN300 ($\Phi = 300\text{mm}$). Solid lines show the fitted behaviour according to our pipe flow model. The fit was done using the data for DN100 tube only.

been utilized to develop improved methods for predicting frictional losses in straight tube flow of fibre suspensions. Especially, the phenomena related to formation of lubrication layer and to transition from laminar plug flow to mixed and fully turbulent flows have been included to the model successfully. As a result we have obtained empirically motivated new pressure loss correlation that is formally reminiscent of the corresponding scaling law for pure Newtonian flows in turbulent flow. Figure (5) shows an example: the experimental data from DN100 pipe alone has been used to predict accurately the pressure loss for two bigger pipes.

4 Effect of fiber and pulp properties on filtration

Filtration of pulp is one of the key processes found in paper machines. Typically, this has been studied by simple and straight-forward means, e.g. by measuring fluid flux and pressure loss through the consolidating fibre layer in a hand-sheet mould or in various dynamic filtration devices. Such studies mostly address bulk properties of the filtrate such as flow resistance and the average degree of consolidation. Instead, they do not give much information on the detailed dynamics of the filtration process itself or on the evolution of the local conditions inside the filtered layer such as density distribution, flow resistance distribution and stress state of the forming fibre network. Such an experimental information would however be invaluable e.g. for analysis and realistic modeling of paper-making processes involving filtration and consolidation of fibres. To address this problem we have

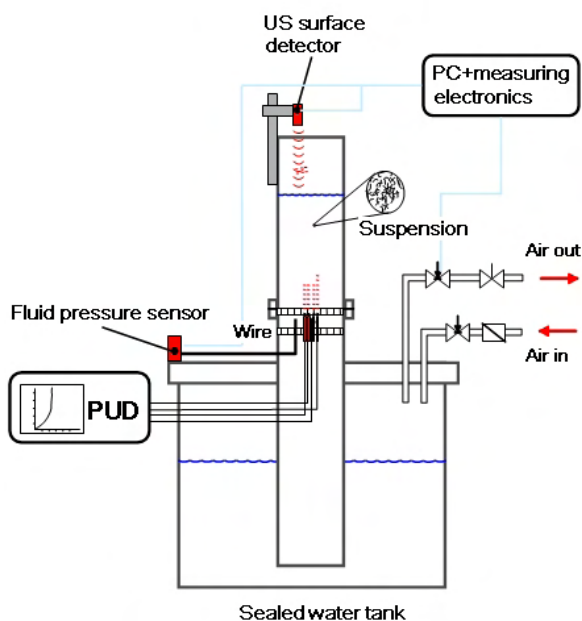


Figure 6: Schematic illustration of the filtration device.

introduced a novel method for measuring the local velocity field of fibres during filtration of dilute liquid-fibre suspension [4]. The device consists of a simple gravity or pressure driven hand-sheet mould equipped with a pulsed ultrasound-Doppler anemometer for measuring the local time-dependent velocity field of the fibre phase during vertical filtration (see Figure (6)). The total flux of the suspension is independently measured using a separate ultrasound transducer to detect the position of the free surface of the suspension in the mould. Pressure loss caused by the consolidating fibre layer is measured by a pressure sensor located under the filtration wire. Using the two-phase flow equations appropriate for the present system, the other relevant flow quantities (fields) such as fluid velocity and pressure, consistency, flow resistance and structural stress of the fibre network can be computed based on the measured data. The method can thus provide detailed information on the dynamics of filtration and material properties of the consolidating fibre layer that has not been previously available.

We have used the filtering device intensively to good effect. By varying the fiber type and properties e.g. by refining or fractioning one has obtained completely new

information of fibrous structures [5,8]. In Figure (7) we show as an example how the measured structural pressure depends on the fiber type and consistency. We have

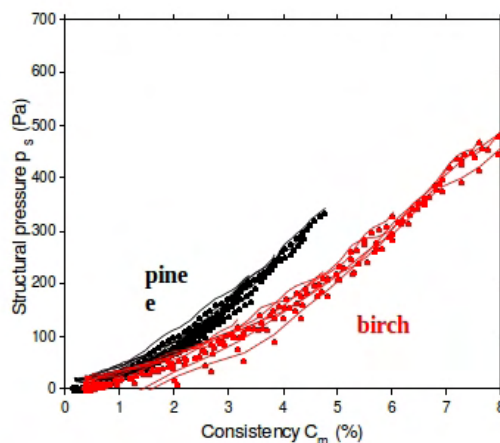


Figure 7: Measured structural stress of the fibre network for a birch and pine pulp as a function of consistency.

recently started developing together with University of Jyväskylä a measurement device for 2D filtration (see Figure (8)). The data obtained will be used for tuning the parameters for a realistic 2D filtering model developed in co-operation with University of Jyväskylä and Numerola corporation. This model will be used for the analysis of forming section, where the pulp is in strongly sheared condition in the initial phase of water removal.

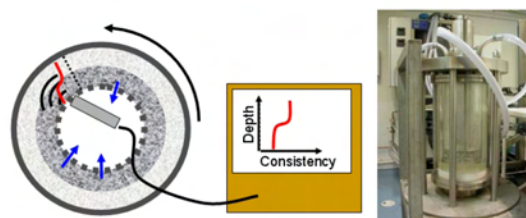


Figure 8: Measurement device for filtration in a 2D shear flow.

5 Mixing of high-consistency pulp suspensions

Many industrial unit operations involved with multi-phase flow systems comprise of flow, agitation and mixing of solid-liquid suspensions both in tanks and pipings. Agitated pulp stock chests are, e.g., used in various mixing operations in pulp and paper industries acting as stock blenders and consistency controllers. Homogeneity of pulp suspension in mixing tanks and pipe lines is essential regarding the performance of the whole pulp and paper manufacturing processes.

Non-ideal phenomena encountered in common pulp chests, such as channelling, recirculation and stagnant zones make the prediction of the agitation performance very challenging. At a very low consistency fibre suspension behaves much like a Newtonian fluid (water). As the consistency increases pulp suspension forms a continuous fibre network having non-Newtonian rheological properties.

We have studied mixing of both sand and pulp in a 160 litre laboratory tank (see Figure (9)). The 3D velocity profiles in the tank were measured using a pulsed

ultrasonic Doppler equipped with a custom made submersible probe (see Figure (9)). The radial measurement locations are illustrated with orange vertical lines in Figure (9). Our measurement results have been used to develop better mixing models for particle suspensions [6]. They have also shown, that for fiber suspensions present models are unable to describe the complex rheological behaviour seen in fiber suspensions (see Figure (9)). Flow and mixing inside a pilot scale (8 m^3)

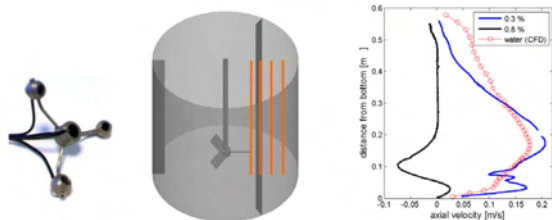


Figure 9: On the left: Submersible 3D-PUDA probe. In the middle: Geometry of the mixing tank. The measurement positions have been shown with orange vertical lines. On the right: Axial time-averaged measured and simulated particle phase velocity components on radial location $r=0.145 \text{ m}$. At lower consistency the fibre suspension behaves like pure water, whereas for the higher consistency the behaviour is dramatically changed. For the higher consistency mixing occurs only very close to the impeller.

mixing tank equipped with a side mixer was studied by measuring the circulation time of RFID tags (see Figure (10)) fed into the pipe mixer side streams [7]. The tracer tags merged into the main flow reappeared in one of the RFID detection zones after passing through the mixing tank. Figure (10) shows a histogram of measured circulation time t^* . The histogram is based on 18,000 RFID tag detections. Here t^* is a dimensionless circulation time obtained by scaling the measured circulation time by the circulation time that would be seen without mixing (plug flow in the tank). We see, that the tag distribution looks close to exponential. This indicates that mixing is pretty good, although there seems to be some channelling of the flow involved.

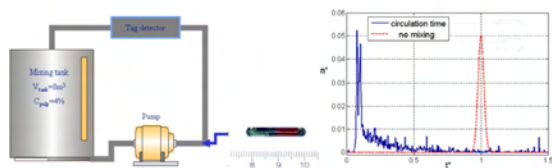


Figure 10: On the left: Experimental setup for measuring circulation time. In the middle: Image of a RFID transponder. On the right: Measured RFID tag circulation time.

6 In-line pipe rheometry for complex slurries

There is a huge number of commercial viscometers and rheometers available. However, there are few that can be used for measuring the rheological behaviour of complex slurries in process-like conditions. There are several problems with current technologies: flow geometries in commercial rheometers are too small for flocculated

suspensions, flow loops demand big sample sizes, pump driven flow has disturbances and pumps have small viscosity/flow range.

To address these problems we have developed a new rheometer (see Figure (11)). The device is based on flow in a vertical pipe connecting two containers. The pressure loss is measured on two locations of the pipe, and the velocity profile inside the pipe is measured simultaneously with a pulsed ultrasound-Doppler anemometer. This approach has two advantages: one is able to resolve the true viscosity of the sample fluid with several shear rates simultaneously, and the effect of slip close to the pipe walls can be eliminated. In Figure (11) we show an

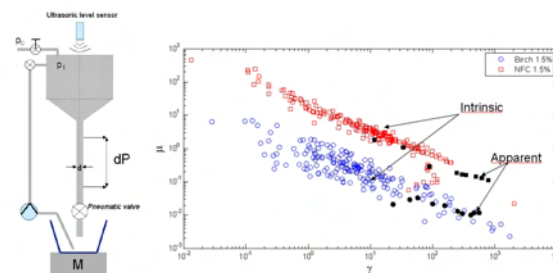


Figure 11: On the left: Experimental setup for measuring circulation time. In the middle: Image of a RFID transponder. On the right: Measured RFID tag circulation time.

example of the results obtained with our new rheometer: the intrinsic (calculated locally on different radial locations) and apparent (calculated globally for the whole pipe by assuming Poiseuille flow) viscosities are shown as a function of shear rate for 1.5% birch and 1.5% nanocellulose. We see from this figure, that both fluids exhibit strong shear thinning behaviour in this shear region.

7 Discussion

Above we have given several examples of our work with fiber suspension rheology. The list is not exhaustive, other interesting topics would have been e.g. the analysis of sedimenting rod-like particle suspensions [10,11], and the initial dewatering at the forming section of the paper machine [12]. The former is a good example how academic basic research can lead to a new innovative industrial concept, and the latter shows how our expertise has been used to develop a new measuring method for analysing a complicated real-life filtering problem.

The roots of our team are in forest industry, but our general rheological expertise and our experimental methods can be easily applied to rheological problems coming from other industrial areas. Already now, a notable fraction of our effort is used outside traditional forest industry.

References

- [1] Karema, H., Salmela, J., Tukiainen, M., Lepomäki, H., "Prediction of paper formation by fluidisation and reflocculation experiments", FRC Symposium on the Science of Papermaking. Oxford, UK, 17–21 Sept. 2001. Fundamental Research Committee (FRC). Oxford (2001), 29 p.
- [2] Salmela, J., Kataja, M., "Floc rupture and re-flocculation in turbulent shear flow", Proc. of Advances in Paper Science and Technology, 13th Fundamental Research Symposium. Cambridge, 11–16 Sept. 2005. FRC, The Pulp & Paper Fundamental Research Society. Cambridge (2005), 15 p.
- [3] Jäsberg, A., Raiskinmäki, P., Kataja, M., "Rheology and flow behaviour of fibre suspensions", , Rheological materials in process

- industry. ReoMaT Final Report. Kataja, Markku (ed.). VTT Tiedotteita - Research Notes 2428. VTT. Espoo (2008), 55–83
- [4] Kataja, M. and HirsilÄä, P. Application of ultrasound anemometry for measuring filtration of fibre suspension. The Science of Papermaking, Transactions of the 12th fundamental research symposium. Vol. 1. Baker, C.F. (ed.). Oxford, September 2001, The Pulp and Paper fundamental Research Society, UK, 2001. Pp. 591-604
- [5] Haavisto, S., “Application of ultrasound anemometry for measuring filtration of fibre suspensions: effect of fibre and pulp properties”, Rheological materials in process industry. ReoMaT Final Report. Kataja, Markku (ed.). VTT Tiedotteita - Research Notes 2428. VTT. Espoo (2008), 84–93
- [6] Haavisto, S., Koponen, A., Syrjänen, J. and Manninen, M., “UDV measurements and CFD simulation to two-phase flow in a stirred vessel”, Progress in Computational Fluid Dynamics Vol.9 Nr.6–7, 375–382, (2009).
- [7] Haavisto, S., Koponen, A., Luukkainen, V.-M., and Salmela, J. , “Experimental study on mixing of high-consistency pulp suspension in stirred tank and in pipe mixer using 3D-udv and rfid”, Proceedings of the 14th Fundamental Research Symposium, Advances in Pulp and Paper Research, Oxford 2009, Fundamental Research Communications, 13th – 18th September 2009.
- [8] Liimatainen, H., Haavisto, Sa., Haapala, A., Niinimäki, J., “Influence of adsorbed and dissolved carboxymethyl cellulose on fibre suspension dispersing, dewaterability, and fines retention”, BioResources. Vol. 4 (2010) No: 1, 321–340.
- [9] El-Sharkawy, K., Haavisto, S., Koskenhely, K., Paulapuro, H., “Effect of fiber flocculation and filling design on refiner loadability and refining characteristics”, BioResources. Vol. 3 (2008) No: 2, 403–424.
- [10] Salmela, J., Martinez, D. M., Kataja, M., “Settling of dilute and semidilute fiber suspensions at finite Re”, AIChE Journal. Vol. 53 (2007) No: 8, 1916–1923
- [11] Madani, A., Storey, S., Olson, J. A., Frigaard, I. A., Salmela, J., Martinez, D. M., “Fractionation of non-Brownian rod-like particle suspensions in a viscoplastic fluid”, Chemical Engineering Science. Vol. 65 (2010) No: 5, 1762–1772
- [12] Puurtinen, A., Salmela, J., Selenius, P. and Koponen, A., “Effect of different parameters on the development of initial dewatering at shoe and blade gap former”, proceedings of Papercon 2010, Hyatt Regency Atlanta, 265 Peachtree Street, Atlanta, GA 30303.
- [13] Hämäläinen, T., Hämäläinen, J., Salmela, J. “Evolution of fibre flocs in a turbulent pipe expansion flow”, 6th International Conference on Multiphase Flow, ICMF 2007. Leipzig, July 9 - 13, 2007. Martin-Luther-Universität Halle-Wittenberg. Leipzig (2007).

STREAK FORMATION AND FIBRE ORIENTATION IN NEAR WALL TURBULENT FIBRE SUSPENSION FLOW

M. Kvick,¹ K. Håkansson,¹ F. Lundell,² L. D. Söderberg,^{1,3} and L. Prahl Wittberg²

¹ Wallenberg Wood Science Center, KTH Mechanics, Royal Institute of Technology, SE-100 44 Stockholm, Sweden

² Linné FLOW Centre, KTH Mechanics, Royal Institute of Technology, SE-100 44 Stockholm, Sweden

³ Innventia AB, SE-114 86 Stockholm, Sweden

kvick@mech.kth.se, karlh@mech.kth.se and fredrik@mech.kth.se

Abstract

In papermaking, the structure and mechanical properties of the final, dry paper are to a large extent determined by the flow of a low concentration ($< 1\%$) cellulose fibre suspension early in the process. A key flow device is the headbox nozzle, a 2D contraction that generates a thin and wide fibre suspension sheet that is jetted out onto permeable forming wires, where the paper is formed. Aiming at understanding how the mass and orientation distributions in the final paper are affected by the flow along internal surfaces of the nozzle, a turbulent fibre suspension flow near a wall is investigated experimentally in this study. The experimental setup consists of an inclined open rectangular channel made of glass with reservoirs in the upstream and downstream position. A pump is used to transfer the suspension from the downstream to the upstream reservoir. The suspension flows down the inclined channel driven by gravity. Cellulose acetate fibres with a density $\rho_f = 1300 \text{ kg/m}^3$ and aspect ratios $r_p = 7, 14$ and 28 are used. The friction Reynolds number is varied between 50 and 230 by adjusting the angle of inclination of the channel and the thickness of the water layer flowing down the channel. By analyzing images taken from beneath, through the glass bottom of the channel, on the fully developed flow, fibres are detected using a steerable filter. The position and orientation of the fibres in the flow parallel plane are obtained and fibre streaks are analyzed by a correlation. The width of the fibre streaks are compared with the empirical value of $\sim 50l^+$ for low velocity streaks in turbulent boundary layers, where l^+ is the viscous length scale. The result show that the fibre streaks scale in the same manner as the viscous sublayer streaks in a turbulent wall bounded flow. It is shown that the fibres do not seem to form streaks for all cases studied. Strong streakiness (as measured by the minimum value of the correlation of the concentration distributions in the spanwise direction) is observed in a certain range of friction and particle Reynolds number. In the case when the streakiness is low, most of the fibres have an orientation aligned with, or close to, the flow direction.

Introduction

In papermaking, the mass and orientation distribution of cellulose fibres, therefore also the mechanical properties of the paper, are highly dependent on the flow in the headbox nozzle. The headbox is a 2D contraction that generates a thin ($\approx 1 \text{ cm}$), wide (up to 10 m) fibre suspension sheet that is jetted out onto permeable forming wires, where the paper is formed.

The highly complex flow in a headbox, where the flow is both turbulent and accelerated, together with the presence of several surfaces, motivates studying the behavior of fibres in turbulent shear flow. An increased understanding of fibres in wall bounded turbulent flow will give a better understanding on the effects of the headbox on the final paper. Not only the distribution of the fibre orientations, i.e. the fibres individual direction in the flow, but also the overall fibre orientation and the distribution of the fibres in the cross direction (spanwise) is of interest. When producing paper, the orientation of the fibres and the basis weight of the paper are the factors that decides the mechanical properties of the paper. The desired properties are in turn determined by the type of product (*e.g.* packaging, newsprint or tissue).

Earlier experiments have been conducted by Carlsson(2009), who mainly investigated orientation and distribution of cellulose fibres in laminar flow. In this study, although the experimental setup is similar to the one used by Carlsson(2009), the emphasis will lie on studying fibres in turbulent shear flow. Jeffery(1922), derived the equations of motion for ellipsoidal particles in inertia less shear flow. He found that the particles rotated in stable orbits, the so called Jeffery orbits. It has been demonstrated experimentally that fibres in shear flow experience these kind of motions.

It is well known that in a turbulent flow, there exists coherent structures in the boundary layer, known as viscous sublayer streaks. These turbulent streaks scale with the viscous length scale l^+ :

$$l^+ = \frac{\nu}{u_{\tau_{wall}}}, \quad (1)$$

where $u_{\tau_{wall}} = \sqrt{\tau_{wall}/\rho}$ (τ_{wall} is the shear stress at the wall and ρ is the density of the fluid) is the friction velocity and ν the kinematic viscosity. Although the exact structure of the turbulent boundary layer streaks is not certain, the width of the streaks has been well investigated and reported to be on average $50l^+$, by *e.g.* Zacksenhouse et al.(2001).

Several experiments and numerical simulations have been performed regarding particles in turbulent boundary layers. Kaftori et al.(1995) studied the deposition of spherical particles in streaks while Nino & Garcia(1996) used both non symmetrical and spherical particles. To the authors best knowledge, experiments regarding formation of fibre streaks in turbulent shear flow has not been conducted earlier. Although, simulations regarding this phenomena exists, *e.g.* Mortensen(2007).

In the present study, fibres in a turbulent wall bounded flow are studied experimentally, effort is put into finding out when fibres gather in streaks. Moreover, the distributions of the fibre orientation are of interest, both for the cases when fibre streaks are and are not present.

Experimental Setup & Analyzing Techniques

The experimental setup, shown in Figure 1(a), consists of an inclined channel made of glass with length 2 m and width 0.56 m. Water is pumped to an upstream reservoir and allowed to flow down the plate driven by gravity alone. Reservoirs are located upstream and downstream of the glass plate in order to reduce disturbances in the flow. Submersible pumps are placed in both reservoirs to stir the suspension and secure that all fibres are circulated in the system. The system requires a liquid volume of 120 l to function properly. At a downstream position where the turbulent flow is fully developed, a CCD-camera is mounted underneath the glass plate to acquire images of the fibre suspension flow from below. The setup makes it possible to alter the angle of the glass plate (α) and the height (h) of the water layer flowing down the plate. The accuracy is $\pm 0.5\%$ and $\pm 0.9\%$ for the angle and the height respectively. The variations of the above parameters are limited by the experimental setup, the angle is varied between $0.03 - 0.2$ degrees and the height between $6 - 12$ mm. The height of the water layer is measured at several positions to ensure that there are no local acceleration of the flow.

Flow situation

One of the most intriguing aspects with this experimental setup is that since the flow is driven by gravity alone and since the gravitational force is balanced by the force from the glass plate, the wall shear stress is obtained as;

$$\tau_{wall} = \rho gh \sin \alpha. \quad (2)$$

The friction Reynolds number is in turn obtained by the height of the water layer h and the friction velocity $u_{\tau_{wall}}$ as:

$$Re_{\tau} = \frac{hu_{\tau_{wall}}}{\nu} = \frac{h\sqrt{gh \sin \alpha}}{\nu}. \quad (3)$$

Note that Re_{τ} can be determined directly from geometrical and liquid properties for this flow case. The friction Reynolds number is varied between $50 - 230 \pm 2.0\%$. Another important dimensionless parameter is the (particle) Reynolds number for the flow around the particle in the shear near the wall:

$$Re_p = \frac{\tau_{wall} l^2}{\rho \nu^2} = \frac{gh l^2 \sin \alpha}{\nu^2}, \quad (4)$$

with values between $100 - 2000 \pm 1.9\%$.

To ensure that the flow is turbulent and fully developed, LDV measurements are performed. These measurements are performed at and around the point of fiber data acquisition (25 cm upstream and 20 cm on each side of the acquisition point). Velocity profiles and u_{rms} profiles for four different positions can be seen in Figure 2(a) and 2(b).

Fibre suspension

The fibre suspension consists of water with density $\rho_{H_2O} = 1000 \text{ kg/m}^3$ and a dilute concentration of cellulose acetate fibres ($0.0008 < nl^3 < 0.0066$ (with low values for short and high for long fibres) where n is the number density of the fibres). The fibres have a density of $\rho_f = 1300 \text{ kg/m}^3$, a diameter of $d_f = 70 \text{ }\mu\text{m}$ and the fibre lengths are $l_f = 0.5 \text{ mm}$, 1.0 mm and 2.0 mm giving aspect ratios of $r_p = 7, 14$ and 28 . Since the density ratio ρ_f/ρ_{H_2O} is greater than unity, the fibres will

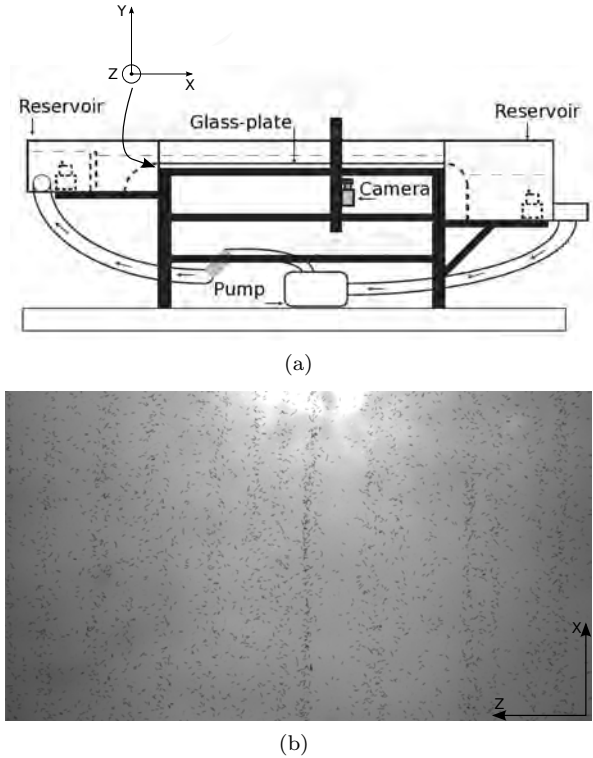


Figure 1: (a) Schematic drawing of the experimental setup. (b) Example of an image acquired during experiment. Fibres have been dyed black for better visibility. The streamwise direction is upward.

sediment in the flow. To increase the visibility of the fibres, the fibres are dyed using a black textile dye (Nitor AB).

Measurement and analysis procedure

A CCD-camera (Prosilica GE-680) and a light source (Drelo Drelloscop 200) placed underneath the glass channel are connected to a computer (MacBook Pro 2.26 GHz Intel Core 2 Duo). By controlling the light source it is assured that the exposure time is short enough for the images to become sharp. The images are acquired using a frequency of $0.14 - 0.30 \text{ Hz}$, depending on the flow velocity, to make sure that the images are statistically independent of each other. For each case, 150 images are acquired. This is found to be sufficient for the streak width and fibre orientation distributions to converge. A typical image is shown in Figure 1(b), where the fibres are black, the streamwise direction is upward. The differences in background intensity is due to surface waves and reflections of the light source. The field of view of is $100 \times 56 \text{ mm}^2$ with a resolution of $1920 \times 1080 \text{ pixel}^2$. The depth of field of the lens used is greater than the depth of the water layer at all times. Hence, all fibres are sufficiently sharp to be detected. The camera settings are kept constant during all experiments.

The images are processed by first subtracting the background noise. The fibres position (x - and z -coordinate in the image), and angle β ($\beta = 0$ in the streamwise direction and $\beta = 90$ in the spanwise direction) are found using a second order ridge detector within the class of steerable filters, Carlsson(2009), Jacob & Unser(1994). The filter has earlier been evaluated by Carlsson(2009), where the effect of noise and unsharpness of the images on the orientation angle were found to be less than 1° for moderate levels of disturbances.

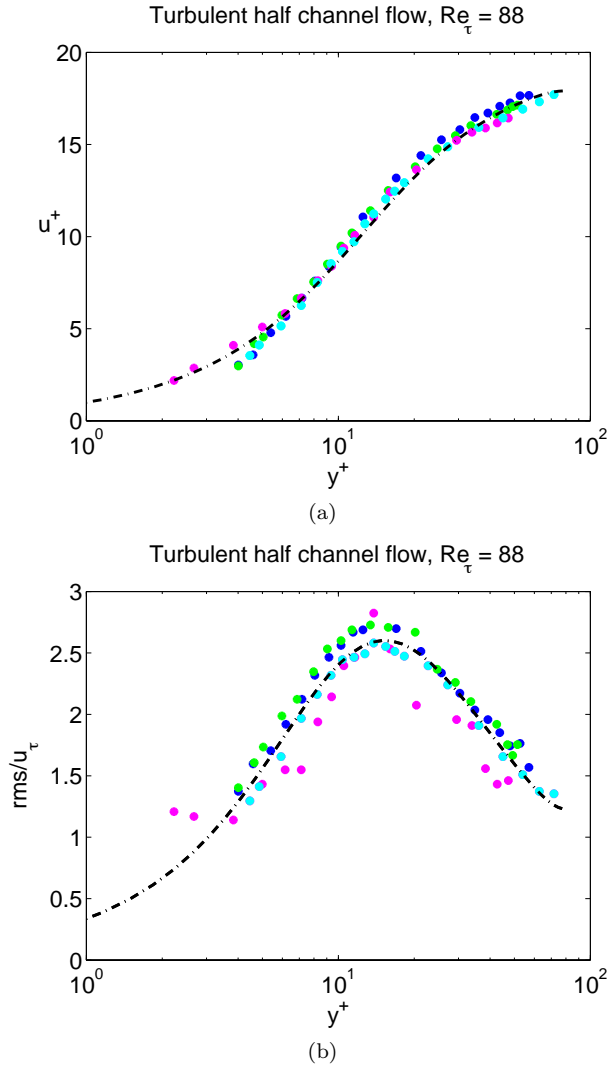


Figure 2: (a) Velocity profiles upstream, besides and at the acquisition point. The dashed line is from DNS of a full channel by [?]. (b) u_{rms} for the same four cases and DNS.

In Figure 1(b), it is clearly visible that the fibres assemble in streaks. This feature is easily determined by the human eye, but is not trivial to study by automatic methods. In this work, the occurrence and width of streaks is measured by the correlation of the spanwise concentration distribution. First, the position of the fibers are used to create artificial fibers with identical orientation. This is done in order to ensure that all fibers are weighted equally in the analysis, regardless of orientation. The intensities of the processed images are summated in the streamwise direction, leading to an intensity distribution graph. For each intensity distribution an autocorrelation is calculated and an average is obtained for all images in the set. The mean streak width is found as the first minimum of the correlation. Since this point is not well defined, in this study the interception point with zero correlation (ΔZ_0) is assumed to be half the mean width of the streaks instead. Similar methods have been used earlier, by e.g. Lagraa et al.(2004). Furthermore, the value of the first minimum of the correlation is taken as a measurement of the streakiness, the lower the minimum, the higher the streakiness.

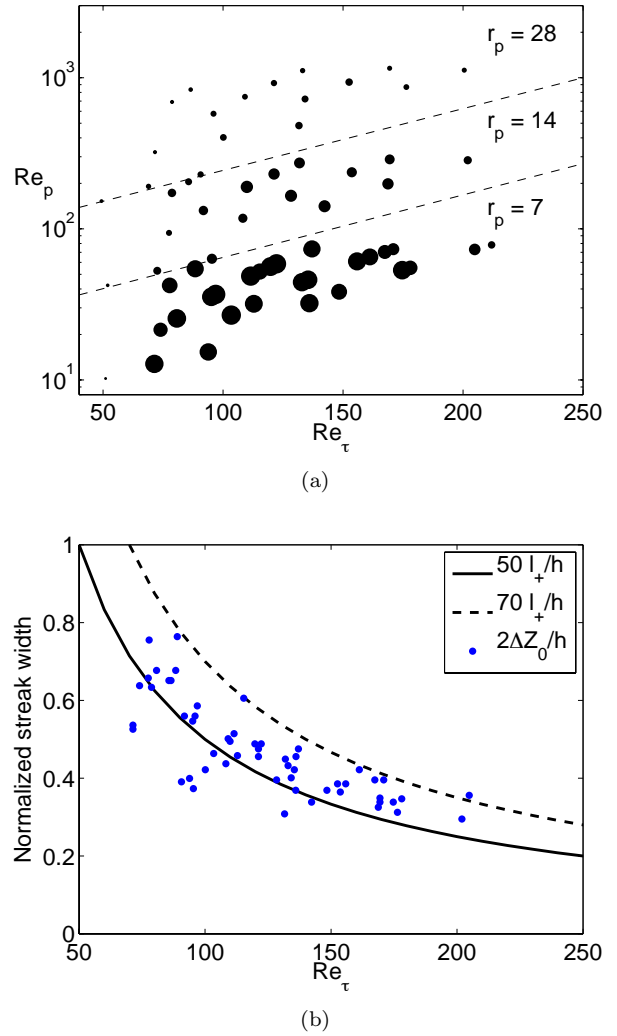


Figure 3: (a) Indication of streakiness, large dots indicate a high streakiness and small dots a low streakiness. (b) Streak width normalized with the height of the water layer versus the friction Reynolds number for all cases with high streakiness.

Results & Discussion

Fibre streaks

In the parameter space investigated, it is of interest to find out when the fibres tend to gather at the surface of the channel and form fibre streaks. In Figure 3(a) the variations of Re_p and Re_τ are shown together with the streakiness. As can be observed from this figure, fibres tend to form streaks for high friction Reynolds number and low particle Reynolds number. Moreover, there are three different regions with no overlap in Figure 3(a). Each region correspond to one aspect ratio and thus the effect of aspect ratio can not be isolated. As is shown in Figure 3(a), the observed streakiness is very low for fibres with aspect ratio $r_p = 28$, while for fibres with aspect ratio $r_p = 7$ most experiments resulted in a high streakiness. Furthermore, depicted in the figure, there is a region where for the same fibre aspect ratio ($r_p = 14$), the streakiness is higher for larger values of Re_τ . Through the comparison of the width of the fibre streaks with the value of $50l^+$, a well known width for turbulent boundary layer low velocity streaks, Figure 3(b) clearly shows that the width of the two types of

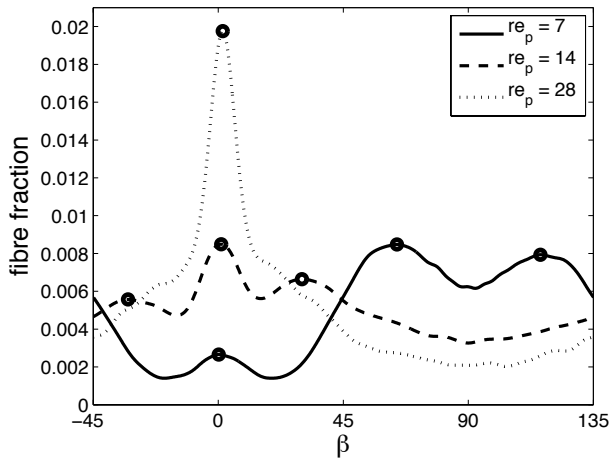


Figure 4: Orientation distribution for $r_p = 7$, $r_p = 14$ and $r_p = 28$. $\beta = 0$ and $\beta = 90$ is in the streamwise and spanwise direction respectively. The distributions are from experiments with $Re_\tau \approx 130$. $Re_p \approx 32$ for $r_p = 7$, $Re_p \approx 165$ for $r_p = 14$ and $Re_p \approx 1113$ for $r_p = 28$.

streaks scale in the same manner, where $2\Delta Z_0/h$ is the streak width obtained from the autocorrelation, normalized with the height of the water layer. Eq. (1) has been used to calculate the viscous length scale l^+ .

At this point, it should be emphasized that in this work, the concentration, as measured by nl^3 , is varied a factor of eight with high values for long fibres ($r_p = 28$). This means that the number density is actually eight times higher for the *short* fibres ($r_p = 7$) as compared to the long ones. This gives a difference of the absolute number of fibres observed in the images and this difference can, by itself, have an impact on the streakiness obtained from the spanwise concentration correlations. These effects are presently under study and will be reported in future work.

Fibre orientation

The fibre orientation distribution is highly dependent on the length of the fibres. Figure (4) show one sample distribution for each aspect ratio; 7, 14 and 28. The distribution for $r_p = 28$ has a large peak at $\beta = 0$ (streamwise) and most fibres are oriented with an angle β between -45 and 45 degrees. Fibres with $r_p = 14$ have a more homogenous orientation distribution, with a peak at $\beta = 0$ and two peaks at $\beta \approx \pm 30$. The fibres with $r_p = 7$ are mostly located in the region $45 < \beta < 135$, for larger Re_p the peak at $\beta = 90$ grows, it is found that this is due to the fact that the fibre orientation is not fully developed for the fibres with the smallest aspect ratio, this is taken into consideration in the analysis. In addition to the results in Figure (4), it is observed that when the streakiness is low the peak at $\beta = 0$ grows for all aspect ratios.

Conclusions

An experimental study has been performed to study the behavior of cellulose acetate fibres in turbulent wall bounded flow. A fibre suspension flowed down an inclined channel driven by gravity, producing a turbulent shear flow. A CCD-camera was mounted below the inclined glass channel to acquire images of the fibres in the flow, and a steerable filter was used to detect the fibres orientation and position in the images. Experiments were performed for three different fibre aspect ratios; the angle of inclination and the height of the water layer were varied. Streaks were quantified by analyzing the autocorrelation of a set of images. It was found that when fibre streaks occurred they scaled in the same manner as the viscous sublayer streaks. However, streakiness was not observed for fibres with $r_p = 28$. Furthermore, streaks could not even be observed by eye. Fibre streaks were formed for high Re_τ and low Re_p .

Investigating fibre orientation distributions it has been found that fibres that do not form streaks tend to have an orientation aligned with, or close to, the flow direction. Streaks formed with $r_p = 14$ fibres had a close to homogenous distribution, while the $r_p = 7$ fibres located in streaks where mostly oriented between 45 and 135 degrees.

Acknowledgements

Thoughts and comments from Dr. Allan Carlsson are greatly acknowledged. The study was funded by Wallenberg Wood Science Center and the Swedish Research Council.

References

- A. Carlsson. Near wall fibre orientation in flowing suspensions. PhD thesis, Royal Institute of Technology, Stockholm, Sweden, 2009.
- M. Jacob and M. Unser. Design of steerable filters for feature detection using canny-like criteria. *Pattern Analysis and Machine Intelligence*, IEEE Transactions on, 26(8):1007-1019, 2004.
- G. B. Jeffery. The motion of ellipsoidal particles immersed in a viscous fluid. *Proceedings of the Royal Society of London. Series A*, 102(715):161-179, 1922.
- D. Kaftori, G. Hetsroni, and S. Banerjee. Particle behavior in the turbulent boundary layer. II. Velocity and distribution profiles. *Physics of Fluids*, 7(5):1107-1121, 1995.
- B. Lagraa, L. Labraga, and A. Mazouz. Characterization of low-speed streaks in the near-wall region of a turbulent boundary layer. *European Journal of Mechanics - B/Fluids*, 23(4):587-599, 2004.
- P. H. Mortensen. Particle dynamics in wall-bounded turbulence. PhD thesis, Norwegian University of Science and Technology, Trondheim, Norway, 2007.
- Y. Ninto and M. H. Garcia. Experiments on particle-turbulence interactions in the near-wall region of an open channel flow: implications for sediment transport. *Journal of Fluid Mechanics*, 326:285-319, 1996.
- T. Tsukahara, Y. Seki, H. Kawamura, and D. Tochio. DNS of turbulent channel flow at very low Reynolds numbers. In *Proc. of the Forth Int. Symp. on Turbulence and Shear Flow Phenomena*, pages 935-940, June 2005.
- M. Zacksenhouse, G. Abramovich, and G. Hetsroni. Automatic spatial characterization of low-speed streaks from thermal images. *Experiments in Fluids*, 31(2):229-239, August 2001.

EULERIAN APPROACH TO MODEL FIBRE ORIENTATION AND FIBRE FLOCCULATION IN PAPERMAKING

H. Niskanen,¹ T. Hämäläinen,¹ J. Hämäläinen¹

¹University of Eastern Finland, Department of Physics Mathematics P.O. Box 1627, FI-70211 Kuopio, Finland.

Abstract

In this paper, two different approaches to model the complex phenomena of fibre suspension flows are presented. One is considering the orientation of fibres, and it is based on diffusion-convection equation for orientation probability distribution and Eulerian model of water flow. The other is accounting the flocculation of fibres and consists of population balance approach combined with two-phase Eulerian model. Numerical examples in papermaking applications are presented for both of the models.

1 Introduction

Paper machine produce paper from wood fibres, fillers and chemicals. In the beginning of paper machine, the headbox distributes the mixture of raw materials and water onto the forming fabrics, where the dewatering starts due to pressure differences obtained by a vacuum roll and fabric tension. The basic fibrous structure and the solid material distribution of the paper sheet are determined here at the wet end of a paper machine. After the forming section, only fines and fillers can move towards the surfaces during pressing, whereas the fibres stay in the positions that they have taken during the forming.

There are basically two features of the paper structure controlled in the wet end: the orientation of the fibres and the distribution of the solid materials, both in three dimensions in the paper sheet. The fibre orientation has a significant influence on the strength properties and dimensional stability of the paper sheet. In addition, curling and cockling of paper under moisture changes depends strongly on the fibre orientation. Furthermore, fibres tend to form aggregates in typical headbox concentrations and this flocculation creates an unwanted variance in the in-plane basis weight distribution of the sheet at millimetre to centimetre scales.

Both orientation and flocculation depend on fluid dynamics in the headbox. Turbulence makes orientation more random and breaks up the fibre flocs, where as the mean velocity gradients orient the fibres and stretches the fibre flocs. In addition, the fibres attenuate turbulence. Thus, the fibre suspension flow has a multi-phase nature with couplings between the phases and turbulence. Understanding all the phenomena related in particle suspensions is essential in controlling the industrial process.

2 Modelling approaches

In general, two distinct approaches can be considered when modelling fluid-particle systems. A Lagrangian approach solves the particle trajectories and fluid-particle interactions directly, whereas Eulerian approach considers the probability of finding a particle at a certain location. For non-spherical particles the interest also lies in

determining the probability of a particular orientation. The Lagrangian approach is limited to small scales; often too small for industrial interest. In those cases, the Eulerian approach is preferred.

2.1 On modelling the fibre orientation

Research concerning the rheology of suspensions and particle orientation has been vivid for decades [1, 2, 3, 4]. The research area covers various fields in industry dealing e.g. with fibres and polymers. The fibre orientation has been a subject of many experimental, numerical and theoretical studies, e.g. [5, 6, 7, 8, 9]. The current understanding is limited to simple shear flows and laminar dilute systems. There is no perfect model to describe the interactions between the fibre phase and the carrying fluid, nor for the balance between the flow acceleration and turbulence. Generally, it is known that turbulence randomises the fibre orientation distribution [5, 6] whereas the presence of the fibres attenuate velocity fluctuations [10]. In addition, flow acceleration orients the fibres in to the flow direction. All these phenomena co-exist in the wet-end and affect the quality of the paper product.

2.1.1 The Fibre Orientation Probability Distribution (FOPD) model

The wood fibres are flexible, and the flow of the suspending fluid is usually turbulent. Thus, the orientation of the fibres used in papermaking is not that unambiguous. The complex flow phenomena present additional challenges in estimating the interactions between the fluid and the fibres.

The motion of a fibre can be considered to consist of translation and rotation. In the fibre suspensions the suspending liquid carries the fibres along the mean flow and the velocity fluctuations induce fibre rotation. Linear flow gradients align fibres in the flow direction whereas velocity fluctuations distract the alignment. One of the earliest studies of the motion of non-spherical particles was done by [11] with his derivation for the motion of an ellipsoidal particle in a simple shear flow. Numerous studies have followed concerning, for instance, direct simulation of particles in turbulent flow [12], the fluid particle systems by means of probability distributions [13] or orientation tensors [2].

The fibre orientation is often described by a probability distribution function [14, 15, 16] and its evolution can be estimated with a diffusion-convection equation

$$\frac{\partial \Psi}{\partial t} - D_t \nabla^2 \Psi - D_r \nabla_{S^2}^2 \Psi + \nabla \cdot (\vec{v} \Psi) + \nabla_{S^2} \cdot (\vec{w} \Psi) = 0. \quad (1)$$

where $\Psi = \Psi(x, y, z, \phi, \theta)$ is the orientation distribution, (x, y, z) is the position and (ϕ, θ) determines the orientation of the particle, as illustrated in Figure (1). Subscript

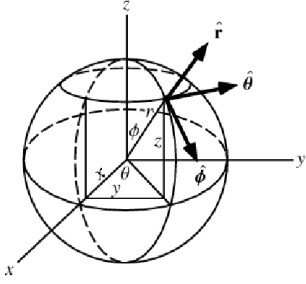


Figure 1: The coordinate system used for the orientation distribution function; a Cartesian coordinate system for spatial parametrisation and spherical coordinates for the orientation vector.

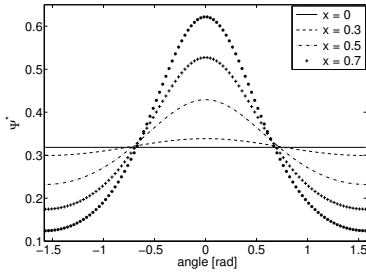


Figure 2: Fibre orientation probability distributions with various positions along the contraction.

S^2 refers to the coordinate system of ϕ and θ . Coefficient D_t and D_r are the so-called translational and rotational diffusion coefficients, respectively. Here \vec{v} is the velocity of the fluid in and $\vec{\omega}$ is the rotational velocity of the fibre defined as

$$\vec{\omega} = \omega p + \lambda \epsilon p - \lambda \langle p, \epsilon p \rangle p, \quad (2)$$

where ω and ϵ are the vorticity and shear strain rate, respectively, and p is unit vector in (ϕ, θ) . The coefficients D_r and D_t can be obtained from experiments through a fitting procedure or estimated from the measured properties of the flow, e.g. kinematic viscosity, dissipation [3, 13] or shear rate [1].

The above method is a somewhat statistical approach to predict the development of the particle orientation distribution. However, the method requires closure approximations in order to be meet physical conditions. Boundary conditions are set depending on the applied geometry.

The FOPD model is solved after determining the velocity profile in the given geometry. At this stage there is only one-way coupling between the orientation distribution and the flow; the flow affects the distribution but not vice versa. However, a model with two-way coupling is being developed (see e.g. [9]).

Figure (2) shows the fibre orientation distributions obtained from the one-dimensional form of Eq. (1) and Eq. (2). In this plot a constant inlet value $\Psi = 1/\pi$ is used, and the velocity profile is from a linearly contracting channel. In general, the higher the flow rate, the greater the probability of a fibre to align with the flow direction, and the smaller the probability for a fibre to be perpendicular to the flow.

The simplified FOPD model can be used for considering the orientation of fibres in a large flow geometry. The model can be employed in a range of flow conditions, including intense turbulence or strong shear flows,

for which it provides statistical information on how the orientation develops on the average.

2.2 On modelling the fibre flocculation

Wood fibres are known to form aggregates even at low concentrations, when the fibres collide and entangle due to the mechanical forces between them [17]. Floc size varies depending on flow conditions, fibre properties and fibre concentration [18]. Moreover, in any given suspension there exists wide distribution of flocs of different diameters. Traditionally, flocculation research has been focused on prediction of the flocculation tendency [19] or the average floc size, but these properties are not sufficient to describe flocculation in paper forming. The occurrence of different floc sizes indicate that the effect of local flow conditions on the floc size distribution must be captured. To simulate a range of floc sizes, one needs a two-fluid approach, water being the carrying phase and the flocs being the dispersed phase. In addition, the dispersed phase needs to be discretized into several size groups so that floc dynamics can be taken into account.

2.2.1 Fibre Floc Evolution (FFE) model

The population balance method combined with an Eulerian two-fluid model form the basis for the Fibre Floc Evolution (FFE) model. For the sake of simplicity, flocs are assumed to be spherical. In the population balance approach one additional conservation equation is solved for each size group, and thus, in order to study ten different particle sizes, for example, ten complementary equations are needed.

Let $N = N(V_m, t)$ represent the number density of particles of size V_m at time t . The population balance equation for the size group V_m then is [20]:

$$\frac{\partial}{\partial t} N + \frac{\partial}{\partial x_i} (N u_d) = B_B - D_B + B_C - D_C \quad (3)$$

where B_B, D_B, B_C and D_C represent the birth rate due to break-up of larger particles, the death rate due to break-up into smaller particles, the birth rate due to coalescence of smaller particles, and the death rate due to coalescence with other particles, respectively. These rates may further be expressed with their own equations which consist of several flow dependent variables and floc dependent parameters. As Eulerian multiphase modelling is utilised for solving the flow field and turbulence, the variables are calculated from the flow field at each iteration step. Turbulence and shear generated by walls and sudden expansions of the geometry, for example, break up the large flocs into the smaller ones, whereas the absence of flow disturbances initiates the coalescence of small flocs into larger ones. In addition, there are certain parameters that depend on the physical properties of the flocs and on the interaction between carrying and dispersed phase.

2.2.2 Numerical examples of flocculation simulations

The FFE model has been validated in a pipe geometry consisting of a 16 mm diameter constriction section 26 mm diameter expansion section. As can be noticed in Fig. Figure (3), the FFE simulations are quite accurate for different flow rates. The model predicts the sudden decrease of local mean floc size immediately downstream of the sudden expansion. Moreover, the model captures

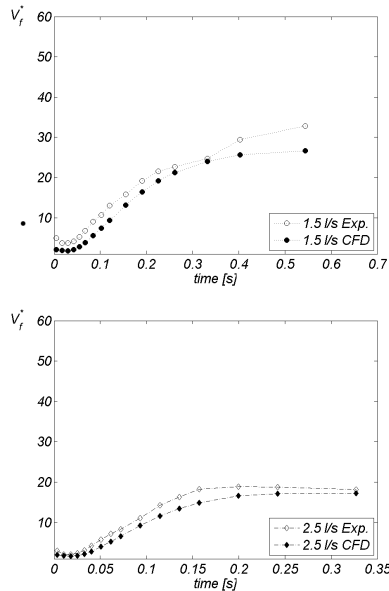


Figure 3: Simulated and measured floc size evolution of pine pulp as a function of the mean residence time for the flow rate of 1.5 l/s. (*left*) and 2.5 l/s (*right*) (experiments by Salmela and Kataja, reported in Ref. [24]).

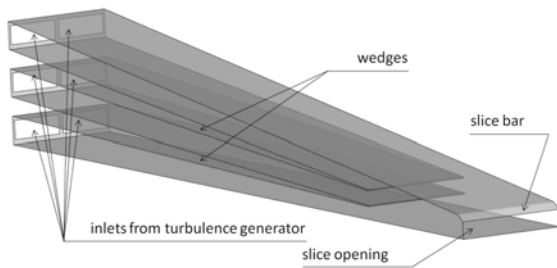


Figure 4: Slice channel with wedges.

accurately the subsequent tendency of increase of the mean floc size, as well as the saturation of the floc diameter at a certain level, which seems to depend on the flow rate. More detailed analyses of the model parameters and the applicability of the FFE model can be found in Refs. [21, 22, 23].

Since the model parameters do not depend on geometry, we may assume that they represent properties of the suspension. Hence, the model is applicable for other parts of the paper machine as well. One example of the utilisation of the FFE model is the slice channel of a headbox, which is typically from 6 to 10 metres wide and 600 mm long. Since the headbox consists of 60 mm wide sections in spanwise direction, it is reasonable to study the fibre flocculation in such a geometry, see Fig. Figure (4). Because there were not any measurements available for the floc size distribution at the inlet of the slice channel, the distribution is set based on the experience.

The evolution of different size groups in the slice channel can be observed in Fig. Figure (5), in which the floc size distribution is illustrated at different locations in the streamwise direction (MD). The positions lie in the middle between the two wedges in vertical direction and in the middle of the outlet of the turbulence generator pipes in the spanwise direction. The numbers in the legend refer to size group category: 1 is the size group of the smallest and 10 is the size group of the largest flocs. In the beginning of the slice channel, the floc size dis-

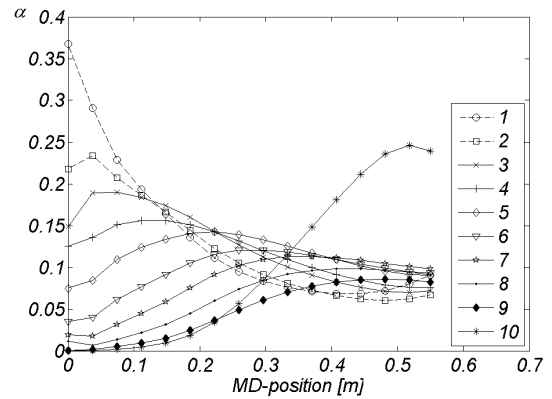


Figure 5: The evolution of different floc size groups inside the slice channel along the line at the middle of the turbulence generator pipe.

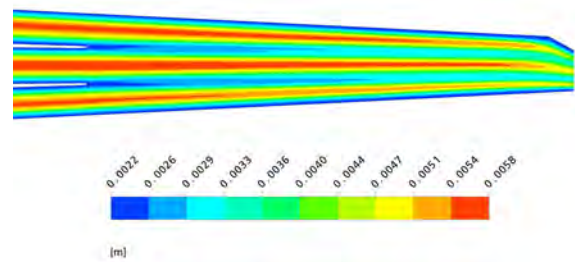


Figure 6: The local mean floc diameter inside the slice channel at the centre plane of turbulence generator pipe; the detail at the end of the channel.

tribution is dominated by the smallest size group, while the biggest two size groups are practically absent. Then, flocs of all sizes start to coalesce and form bigger flocs, but the process still remains rather calm. In addition, the coalescence occurs in such a way that small flocs do not coalesce to very big flocs instantaneously, but instead they form little larger flocs, which in turn, form again somewhat larger flocs.

It is also interesting to examine evolution of the mean floc size between the wedges. Figure Figure (6) shows that the floc size is smaller near the walls, which is due to the shear layer near the wall. The distance between the wedges is not exactly the same, which causes the differences in the contour: The floc size is large in the larger volume in the middle gap than in the top and the bottom gaps.

3 Conclusions

The presented Eulerian models offer an interesting possibility for investigation of fibre suspensions at industrial scale, since they aim at considering the real behaviour of these complex fluids. However, the models neglect the two-way coupling between water and fibres or flocs. In addition, the dependency of the model parameters on different pulps and concentration of the suspension are not determined yet. Therefore, further model development is required in order to describe the phenomena more rigorously.

The current FOPD model can rather well predict the development of the most probable fibre orientation in bulk flow. However, there is e.g. the singularity problem which limits the application of the model at the moment and enforces the use of simplifications. Naturally, mod-

elling always requires simplifications and sometimes it is not possible to include all the features of the modelled problem due to the computational costs, for example. Thus, the use of CFD with somewhat statistical approach is a neat compromise in order to provide necessary information for many industrial problems.

Although the FFE model is able to account the effect of local flow conditions to the floc size distribution at least qualitatively correctly, more experimental data would be needed to further develop the model. It is known that pulp properties affect flocculation mechanisms and resulting solid material distribution on a paper sheet, but the details remain still unknown. FFE model offers however an auspicious basis for the development of papermaking processes, since it is relatively easy to implement and usable in pilot scale geometries as well.

References

- [1] F. Folgar and C.L. Tucker III. Orientation behaviour of fibers in concentrated suspensions. *J.Reinf. Plast. Compos*, 3, 1984.
- [2] S.G. Advani and C.L. Tucker III. The use of tensors to describe and predict fiber orientation in short fibre composites. *J. Rheology*, 31(8), 1987.
- [3] J. A. Olson and R. J. Kerekes. The motion of fibres in turbulent flow. *J. Fluid Mech.*, 377:47–64, 1998.
- [4] C.J.S. Petrie. The rheology of fibre suspensions. *J.Non-Newton Fluid Mech*, 87(2-3):369–402, 1999.
- [5] O. Bernstein and M Shapiro. Direct determination of the orientation distribution function of cylindrical particles immersed in laminar and turbulent shear flows. *J. Aerosol Sci.*, 25(113), 1994.
- [6] E. Krushkal and I Gallily. On the orientation distribution of non-spherical aerosol particles in general shear flow part 2. the turbulent case. *J. Aerosol. Sci*, 19(2):197–211, 1988.
- [7] J.A Olson, I. Frigaard, C Chan, and J. Hämäläinen. Modelling turbulent fibre suspension flowing in a planar contraction: The one-dimensional headbox. *Int.J. Multiphase Flow*, 30:51–66, 2004.
- [8] M. Parsheh, M.L. Brown, and C.K. Aidun. Variation of fiber orientation in turbulent flow inside a planar contraction with different shapes. *Int. J. Multiphase Flow*, 32:1354–1369, 2006.
- [9] P.J. Krochak, J.A. Olson, and M. Martinez. Fiber suspension flow in a tapered channel: The effect of flow/fiber coupling. *Int. J. Multiphase Flow*, 35:676–688, 2009.
- [10] M. Shin and D.L. Koch. Rotational and translational dispersion of fibres in isotropic turbulent flows. *J.Fluid Mech.*, 540:143–173, 2005.
- [11] G. B Jeffery. The motion of ellipsoidal particles immersed in a viscous fluid. *Proc. Royal Soc., A* 102:161–179, 1922.
- [12] P.H. Mortensen, H.I. Andersson, J.J.J Gillissen, and Boersma B.J. Dynamics of prolate ellipsoidal particles in turbulent channel flow. *Phys. Fluids*, 20, 2008.
- [13] J.A Olson. The motion of fibres in turbulent flow, stochastic simulation of isotropic homogenous turbulence. *Int.J. Multiphase Flow*, pages 2083–2103, 2001.
- [14] R.L. Schiek and E.S.G Shaqfeh. A nonlocal theory for stress in bound, brownian suspensions of slender, rigid fibres. *J.Fluid Mech.*, 296:271–324, 1995.
- [15] M. Parsheh, M. Brown, and C. Aidun. On the orientation of stiff fibres suspended in turbulent flow in planar contraction. *J.Fluid Mech.*, 545:245–269, 2005.
- [16] M. Hyensjö. *Fibre Orientation Modelling Applied to Contracting Flows Related to Papermaking*. PhD thesis, Royal Institute of Technology, Stockholm, 2008.
- [17] S.-G. Mason. Fibre motion and floccation. *Pulp and Paper Magazine of Canada*, 55(13):96–102, 1954.
- [18] H. Karema, J. Salmela, M. Tukiainen, and H. Lepomäki. Prediction of paper formation by fluidisation and reflocculation experiments. In *12th Fundamental Research Symposium*, pages 559–589, 2001.
- [19] M. Steen. *Turbulence and Flocculation in Fibre Suspensions*. PhD thesis, University of Trondheim, 1990.
- [20] *ANSYS CFX-11.0 electronical manual*.
- [21] T. Hämäläinen. *Modelling of Fibre Orientation and Fibre Flocculation Phenomena in Paper Sheet Forming*. PhD thesis, Tampere University of Technology, 2008.
- [22] T. Hämäläinen and J. Hämäläinen. Fibre floc evolution model, part i: Flocculation in a headbox. *Nordic Pulp and Paper Research Journal*, 25(1):39–47, 2010.
- [23] T. Hämäläinen and J. Hämäläinen. Fibre floc evolution model, part ii: Influence of the jet-to-wire ratio to resulting fibre floc evolution in the initial drainage zone. *Nordic Pulp and Paper Research Journal*, 25(1):48–55, 2010.
- [24] T. Hämäläinen, J. Hämäläinen, and J. Salmela. Evolution of fibre flocs in a turbulent pipe expansion flow. In *6th International Conference on Multiphase Flow (CD-proceedings)*, 2007.

ORIENTATION OF FIBERS IN DIFFERENT CONTRACTION PROFILES

Putkiranta M.¹, Eloranta H.¹, Pärssinen T.², Saarenrinne P.¹

¹Tampere University of Technology P.O. Box 589, 33101 Tampere, Finland

²Metso Paper Inc. P.O.Box 587, 40101 Jyväskylä, Finland

Corresponding author: maria.putkiranta@tut.fi

Abstract

In this study we have measured the fiber orientation probability density functions of natural wood fibers and rayon fibers in three channel profiles. The contraction ratio of all the channel profiles is 6:1, but this is achieved with different streamwise acceleration profiles. Results show clear differences between fiber types and channel profiles. The highest fiber orientation anisotropy is obtained in a profile with a non-uniform exponentially increasing level of acceleration.

1 Introduction

Fiber orientation is one of the key parameters as we think of the physical properties of fiber based materials. Strength properties are substantially dependent on fiber orientation anisotropy. Also the dimensional stability of a paper is affected by small and large scale fiber orientation variations. In practice, high contraction ratio in the headbox and adequate jet-to-wire speed difference are the means to achieve higher orientation anisotropy. Starting from the days of Jeffery [1], theoretical understanding of fiber suspension dynamics and fiber-flow interaction has been in the focus of many researchers. Increased computational capacity has also increased the number of modeling and simulation work in the area and increased the need for experimental investigations. Still, the number of experimental work is fractional compared to theoretical. The most often referred experimental studies in the field include the publications of Ullmar [2] and Zhang [3]. Also the publications of Parsheh et al. [4] and Krochak et al. [5] present experimental studies of rigid fibers in planar contractions either to compare or fit the data with a Fokker-Plank type equation. In this work, we study experimentally the orientation distribution of four different fiber types in three channel designs. The study of Parsheh et al. [6] investigates the effect of contraction shape on the orientation of stiff fibers. Motivation of this work is to show how the channel profile may affect the orientation of flexible fibers.

2 Experimental setup

The flow channels used in the experiments are made of 15mm-thick Plexiglas plates. The contraction is 700mm long in channels *C1* and *C2* and 350mm in the channel *C3*. The channel inlet height is 185 mm and the outlet height is 30 mm in all the cases. Thus, a contraction ratio of 6:1 is obtained in all the channels. The differences lie in the streamwise acceleration profile. The channel height profiles are depicted in Figure (1), which also portrays the mean streamwise velocity gradients, dU/dx , based on potential flow estimate at the given flow rate.

C1 is designed to obtain a constant dU/dx along the contraction and *C2* is a simple planar contraction profile. *C3* is also a constant dU/dx profile, but due to the short contraction length, the dU/dx is doubled compared to the level in *C1*.

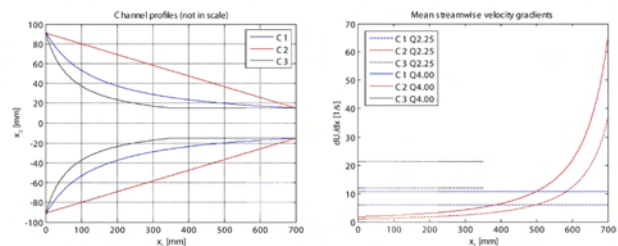


Figure 1: Channel profiles *C1*, *C2* and *C3* and mean streamwise velocity gradients.

A turbulence generator with circular holes of 12 mm in diameter is located in the channel inlet. The turbulence generator produces desired flow conditions, including an even velocity profile in x_2 -direction and high turbulence intensity to randomize the fiber orientation at the inlet. The turbulence generator is located 150 mm upstream of the contracting section.

The channel is installed to a closed flow loop, where water containing fibers is circulating. Two different flow rates, 2.25 l/s and 4.0 l/s, are used to study the fiber orientation at different levels of dU/dx in the same profile.

Four type of fibers are used in the experiments; two length fractions of stiff rayon fibers and two type of real wood fibers; pine and eucalyptus. Length weighted average lengths of the fibers are 4.95 mm and 1.61 mm for rayon, 2.26 mm for pine and 0.75 mm for eucalyptus. Real wood fibers are prepared from pulp sheets by soaking, stirring the mixture to break up the flocks and diluting to the final concentration, which is 0.02% by weight. This dilute suspension allows for clear optical access to the channel center plane. Furthermore, the fiber-fiber interactions and flocculation are avoided and it is assumed that flow state is not affected by the fiber type.

The fibers suspended in the flow are imaged in a back-lighting setup, which is shown in Figure (2). The light source, a Cavilux Smart diode laser with a diffusive back-illumination optics coupled to the fiber optical light guide, is placed to the opposite side of the channel as the camera. The camera is focused into the channel middle plane. At each position, 500 images are recorded and analyzed using the procedure described in the next section. Examples of the image data illustrating both rayon and pine fibers in water are presented in Figure (3). Measurements are done at every 100 mm in channel *C1* and at every 50 mm in channel *C3*. In the upstream half

of the channel $C2$ fiber orientation is measured at every 100 mm and in the downstream half at every 50 mm to obtain better resolution at high dU/dx values.

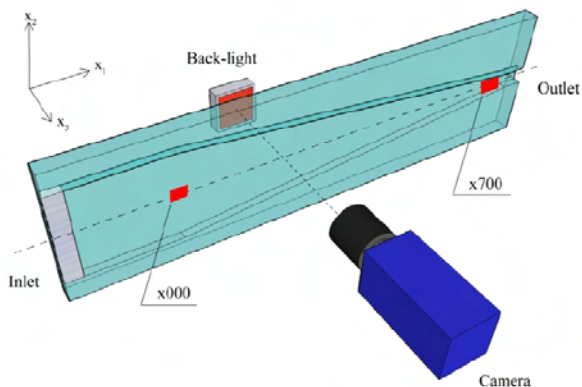


Figure 2: The measurement setup.

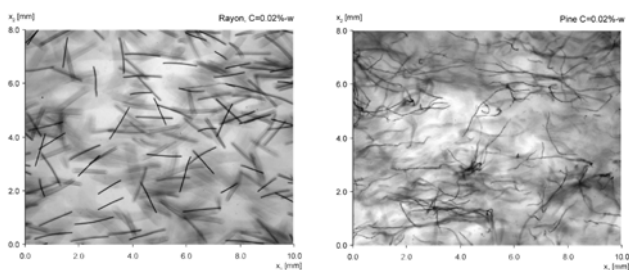


Figure 3: Example images of rayon ($Ll=1.61$ mm) and pine fibers.

3 Data processing

The analysis of the fiber image data follows the procedure originally proposed in Eloranta et al [7]. The images are corrected for uneven illumination by estimating the background and normalizing with the estimate. After that, the images are high-pass filtered to enhance the fibers. In the orientation analysis, the image is divided into subregions with a diameter of 0.5mm. The orientation distribution within each subregion is computed with a Radon-transform, which in essence corresponds to computing line integrals in all the directions. In the case that the fibers are aligned in the direction of integration, a large value of the integrand is expected. The orientation distribution is defined in the range of $-90 \dots +90$ deg with 0 deg corresponds the streamwise, i.e. $x1$ -direction. The Radontransform is a 2D-matrix with the integration angle on the x -axis and location of the integration line on the y -axis. Information on the integration location can be neglected and the local orientation function is obtained by searching for the maximum values in each orientation angle. Finally the procedure calculates the mean orientation distribution over the entire image area by averaging over all the subregions and then over the entire image set. As a result, a normalized orientation PDF at each measurement location is obtained.

Figure (4) illustrates the development of orientation PDFs in the streamwise direction for pine fibers in channel $C2$. A totally random fiber orientation distribution would result in a horizontal line at $p=1/180$. As can be seen, the orientation at the contraction inlet is not

totally random, but nearly random. To facilitate the interpretation of the results the orientation anisotropy is calculated from each PDF by dividing the probability of 0 deg by the probability of 90 deg.

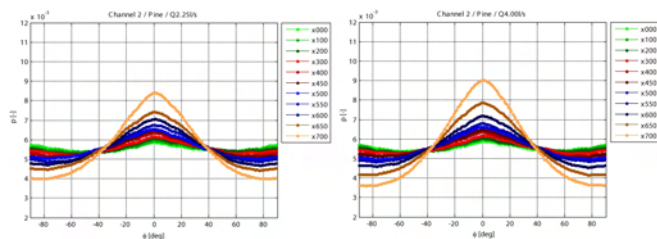


Figure 4: Fiber orientation probability density functions for pine in channel $C2$.

4 Results and discussion

The fiber orientation anisotropy, i.e. $O(x1)/O(x2)$, is presented as a function of the measurement position $x1$ in channels $C1$, $C2$ and $C3$ in Figure (5). In the lower right, the orientation anisotropy in the channel $C2$ is also presented as a function of the local channel contraction ratio C . Local contraction ratio is defined as a ratio of the local mean streamwise velocity to the mean streamwise velocity at the contraction inlet. Naturally, for the profiles $C1$ and $C3$ plotting against C does not change the shape of anisotropy curves, since C is linearly dependent of $x1$. As can be seen, the orientation anisotropy is not dependent only on the local contraction ratio, as the analysis of Olson [8] indicates. He also stated that the fiber orientation is independent on flow rate, which does not seem to hold for real wood fibers. Orientation anisotropy of euca and pine fibers is higher at higher flow rate in every channel profile. It is also obvious from Figure (5), that the shape of the channel profile and fiber properties have a significant effect on the final fiber orientation. It is not only the fiber length, which must be taken into account.

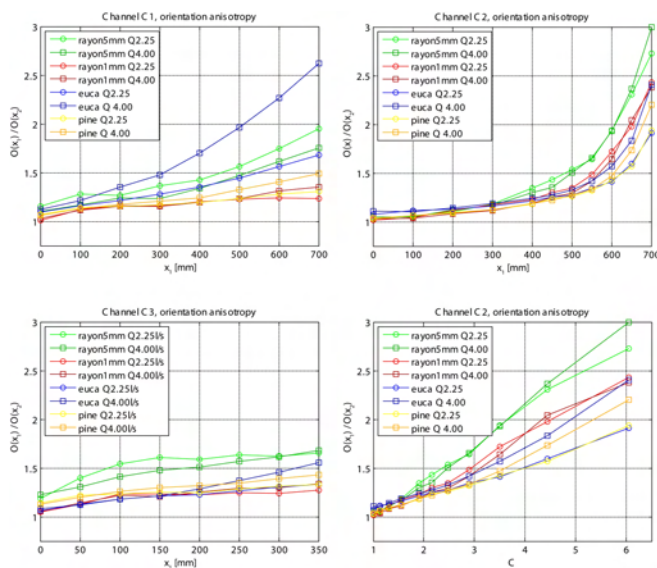


Figure 5: Orientation anisotropy in channel profiles $C1$, $C2$ and $C3$

As can be seen, the channel $C2$ produces the highest orientation anisotropy in almost all the cases, which is contrary to Parsheh et al. [6]. Their numerical results

show, that a contraction with flat walls has the smallest anisotropy at the outlet. They tested their model in constant rate of strain, linear rate of strain and quadratic rate of strain profiles, but they had experimental data only from a profile with flat walls. The only exception in our results is euca in profile *C1* at higher flow rate, where the final anisotropy of euca fibers is higher than in channel *C2*.

Eucalyptus fibers seem to have the biggest difference in anisotropy between the flow rates in all channels. Length weighted average width of eucalyptus is $12\mu\text{m}$, whereas it is around $20\mu\text{m}$ for all the other fibers. It can be assumed, that eucalyptus is more flexible than the other fibers. Pine and eucalyptus fibers are both curly and bent, whereas rayon fibers are more or less straight or only slightly bent in the inlet of the channel (see Figure (3)). As the flow rate is increased, the forces acting on a fiber are increased. As a result, more flexible fibers may straighten more than the stiffer ones.

The results for *C1* and *C3* are interesting, since the level of dU/dx in *C3* is twice the level in *C1*, but it does not result in higher orientation anisotropy. In the profile *C2* both streamwise velocity gradient and acceleration are remarkably higher than in *C1* and *C3*. It can be speculated that in a certain range velocity gradient or acceleration of the flow is not sufficient to result in clear differences in fiber orientation, but in this range the randomizing effect of turbulence and fiber inertia are decisive. To explain the differences between channels *C1* and *C2*, a study of turbulence quantities and scales is probably needed. Different channel profiles also result in different residence time of fibers in the channel. Fibers flow fastest through the channel *C3* and slowest through *C2*, in which fibers stay almost three times longer. The fibers in the measurement are inertial, whereas Olson [8] and Parsheh et al. [6] studied the motion of inertialess fibers, which may explain some of the differences between the results.

5 Conclusions

We have studied the development of fiber orientation in the channel flow with varying streamwise acceleration profiles. There are significant differences between fiber types and flow acceleration profiles in the development of fiber orientation anisotropy and in the final orientation anisotropy at the end of the channel. The main results of this study are:

- The fiber type plays a major role in the development of fiber orientation distribution. Also other fiber properties, not just fiber length, clearly affect the

fiber orientation.

- The channel acceleration profile has a significant effect on the final fiber orientation. Highest anisotropy is achieved in the channel with flat walls, in which the streamwise velocity gradient is increasing exponentially.
- The orientation anisotropy is not dependent only on the local contraction ratio. Especially for real wood fibers the flow rate is also an important factor, which indicates a stronger contribution from the mean flow gradients and turbulence.

Many observations in this work are contrary to what has been presented in two earlier, theoretical studies. In those studies fiber inertia was neglected, the fibers were stiff and turbulent dispersion was either neglected or taken into account.

The results presented here propose a complex relationship between mean flow gradient and the fiber orientation anisotropy. It seems that a high level of acceleration over a short period of time will induce high level of orientation. Mild streamwise acceleration distributed over a longer distance does not cause such a clear response in the fiber phase. In the latter case, turbulence and fiber inertia may be decisive. However, more experimental work is needed to explain these observation and the differences between these results and the earlier studies comprehensively.

References

- [1] Jeffery G., "The motion of ellipsoidal particles immersed in a viscous fluid", Proceedings of the Royal Society London A102: 1922, 161-179.
- [2] Ullmar M., "On Fiber Alignment Mechanisms in a Headbox Nozzle". Licenciate thesis, Royal Institute of Technology, 1998, Stockholm.
- [3] Zhang X., "Fibre orientation in a headbox", Master's thesis, 2002, University of British Columbia.
- [4] Parsheh M., Brown M. L., Aidun, C. K. "On the orientation of stiff fibres suspended in turbulent flow in a planar contraction", Journal of Fluid Mechanics 2005, 545: 245-269
- [5] Krochak P. J., Olson J. A., Martinez D. M. "The orientation of semidilute rigid fiber suspensions in a linearly contracting channel", Physics of Fluids, 2008, 20:073303.
- [6] Parsheh M., Brown M. L., Aidun C. K. "Variation of fiber orientation in turbulent flow inside a planar contraction with different shapes", International Journal of Multiphase Flow, 2006, 32:1354-1369.
- [7] Eloranta, H., Saarenrinne, P., Pärssinen, T., "Estimation of fiber orientation in pulp-suspension flow", Proceedings of the 3rd International Symposium on Two-Phase Flow Modelling and Experimentation, 2004, Pisa, Italy
- [8] Olson J. A., "Analytical estimate of fiber orientation distribution in a head box flow", Nordic Pulp and Paper Journal 2002, 17:302-306.

MODELLING FIBRE SUSPENSION FLOW USING A CONTINUUM APPROACH EXPERIMENTAL CHARACTERIZATION AND SIMULATION

M. Graça Rasteiro^{1,2}, Fernando A.P. Garcia¹, Paulo J. Ferreira¹, Carla A.F. Ventura¹

¹ University of Coimbra, Chemical Engineering Department, Portugal

Research Centre on Chemical Processes and Forest Products Engineering

²To whom correspondence should be addressed: mgr@eq.uc.pt

1 Introduction

The correct design of piping transport systems for pulp fibre suspensions in the pulp and paper mills remains an important issue, mainly because of the high energy consumption involved. However, due to the pulp fibre suspensions complexity it is not yet possible to have a model based on fundamental principles for the design of such systems.

It is known that, contrarily to what happens in the usual solid/liquid suspensions, the components of the pulp fibre suspensions (fibres, fines, etc.) are able to develop new “suspension structures”, which modify the suspension nature and consequently the fluid mechanics characteristics [1], as a result of interparticle forces particularly at intermediate and high consistencies. The fibres have a dampening effect on the turbulence intensity and this intensity decreases as the consistency increases; this effect gradually decreases as the flow rate increases and the fibre concentration has almost no effect if the velocity is high enough [2].

The flow mechanisms of pulp fibre suspension in pipes have been associated with three different regimes with well defined shear mechanisms, as can be seen in Figure (1) where pressure drop ($\Delta P/L$) is plotted against velocity.

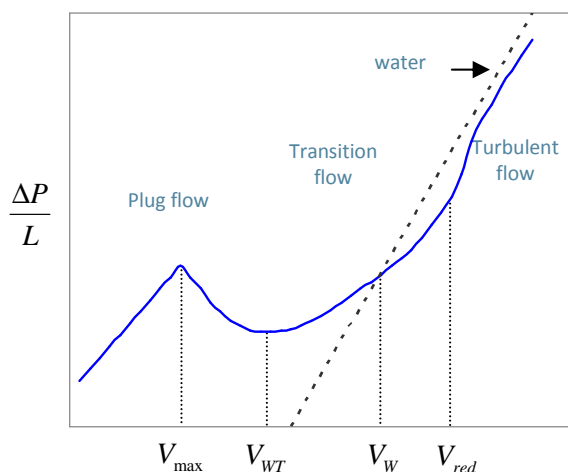


Figure 1: Pressure drop curve for pulp suspensions (adapted from (3-7)).

At low velocities the suspension flows as a plug of fibres and water, and the entire shear occurs in a thin layer adjacent to the pipe wall, where the velocity pro-

file overlaps the one of single phase flow, independent of the fibre concentration [2]. This induces larger values for the suspension pressure drop in pipes than those of water. V_{max} is the velocity corresponding to the maximum of the head loss curve at the plug flow. At intermediate velocities, there is a transition regime where a central and intact plug is surrounded by a turbulent fibre-water annulus. This regime is termed as the transition flow regime, and it starts at the onset of the drag reduction effect, corresponding to a velocity V_W . At high velocities, all the suspension components are in complex turbulent motion, and the pressure drop values are now smaller than the ones expected for water [3-7]. V_{red} is the velocity corresponding to the maximum of drag reduction.

The construction of a flow model able to predict the flow behaviour of pulp fibre suspensions represents an important step in this area, since having access to an accurate modelling strategy can reduce the costs of experiments and prototype equipment to design conveying systems. Some recent attempts have started appearing for extremely dilute suspensions [8].

The team involved in the present work has been carrying out studies at two levels:

- firstly to obtain accurate rheological data for fibre suspensions with different consistencies and for different types of fibres;
- secondly, to model the turbulent flow of pulp fibre suspensions in pipes, by the use of a computational fluid dynamics code (CFD) based on the finite elements method (FEM), and to compare the obtained pressure drop results with experimental data.

Moreover, the experimental validation of fibre flow models is essential in further developments towards a more sound description of flow mechanisms [9]. At the first level, the team has produced an extensive data base of rheological information for short and long bleached Kraft pulp suspensions, by using a new rotational viscometer specially designed for pulp suspensions characterization [10]. The experimental rheograms were adjusted to the Herschel-Bulkley model. The dependence of the rheological parameters on temperature, fibre length and pulp consistency has been studied and the relative influence of these factors on the rheological parameters has been evaluated [11].

At the second level, the $k - \epsilon$ Turbulence Model which is one of the simplest and most used turbulence models for industrial applications, was the selected model in this research. Despite of its large application, this model is based on some restrictions, the most important of which

are that the Reynolds number is high enough and that the turbulence is uniform within boundary layers, which means that production equals dissipation [12]. These assumptions limit the model's accuracy, since they are not always completely followed.

In the results reported here the suspension is described as a pseudo-homogeneous one phase fluid. Moreover, the turbulence parameters in the $k - \epsilon$ model have been taken as a function of fibre type and concentration. The CFD modelling strategy made use of the COMSOL Multiphysics Software version 3.4.

In the following sections the governing equations used in the model will be described, and a discussion of how the turbulence parameters used to simulate the turbulent flow of the fibre suspensions in the pipe had to be adapted according to the fibres type and consistency, will be presented. Moreover, it will be shown how those parameters correlate well with the suspension consistency and, to some extent, with the fibre characteristics.

2 Governing Equations

The $k - \epsilon$ model is used with the Navier-Stokes equations, presented below in its general formulation, considering that the fluid is incompressible [12-13]: Continuity equation – represents the conservation of mass:

$$\nabla \cdot u = 0 \quad (1)$$

Vector equation – represents the conservation of momentum:

$$\rho \frac{\partial u}{\partial t} + \rho(u \cdot \nabla)u = -\nabla p + \nabla \cdot \nu \left(\nabla u + (\nabla u)^T \right) + F \quad (2)$$

Energy equation – represents the conservation of energy:

$$\rho C_p \left(\frac{\partial T}{\partial t} + (u \cdot \nabla)T \right) = -(\nabla \cdot q) + \tau : S - \frac{T}{\rho} \frac{\partial \rho}{\partial T} \left(\frac{\partial p}{\partial t} + (u \cdot \nabla)p \right) + Q \quad (3)$$

where u is the velocity vector (m/s), ρ is the density (kg/m^3), p is the pressure (Pa), τ is the viscous stress tensor (Pa), F is the body force vector (N/m^3), C_p is the specific heat capacity at a constant pressure (J/kgK), T is the absolute temperature (K), q is the heat flux vector (W/m^2), Q contains the heat sources (W/m^3) and S is the strain rate tensor: $S = \frac{1}{2} \left(\nabla u + (\nabla u)^T \right)$. In the present case temperature has been considered constant.

The $k - \epsilon$ Turbulence Model, which is extended to non-Newtonian fluids by allowing the dynamic viscosity to be a function of the velocity field, introduces two additional transport equations and two dependent variables: the turbulence kinetic energy, k , and the turbulence dissipation rate, ϵ . Turbulent viscosity is modelled by:

$$\nu_T = \rho C_\mu \frac{k}{\epsilon} \quad (4)$$

where c_μ is a dimensionless model constant. The transport equation for k can be written by analogy with the equations for Reynolds stresses:

$$\rho \frac{\partial k}{\partial t} - \nabla \cdot \left[\left(\nu + \frac{\nu_T}{\sigma_k} \right) \nabla k \right] + \rho U \cdot \nabla k = \frac{1}{2} \nu_T \left(\nabla U + (\nabla U)^T \right)^2 - \rho \epsilon \quad (5)$$

An equation for ϵ can be derived in a similar manner, though it is impossible to model it on a term-by-term basis. Instead, all the terms that do not have an equivalent term in the k equation were discarded.

$$\rho \frac{\partial \epsilon}{\partial t} - \nabla \cdot \left[\left(\nu + \frac{\nu_T}{\sigma_\epsilon} \right) \nabla \epsilon \right] + \rho U \cdot \nabla \epsilon = \frac{1}{2} C_{\epsilon 1} \frac{\epsilon}{k} \nu_T \left(\nabla U + (\nabla U)^T \right)^2 - \rho C_{\epsilon 2} \frac{\epsilon^2}{k} \quad (6)$$

The model constants in the aforementioned equations are empirical, and their values can be seen in Table (1). Additionally, specific values for the two turbulent quanti-

Constant	C_μ	$C_{\epsilon 1}$	$C_{\epsilon 2}$	σ_k	σ_ϵ
	0.09	1.44	1.92	1.0	1.3

Table 1: Model Constants [12-13]

ties, k and ϵ where required. Alternatively, a turbulence length scale, L_T , and a turbulence intensity scale, I_T , could be specified, which are related with the turbulent variables as follows:

$$k = \frac{3}{2} (|U| I_T)^2 \quad (7)$$

$$\epsilon = C_\mu^{3/4} \frac{k^{3/2}}{L_T} \quad (8)$$

where C_μ has been previously specified and $|U|$ is the mean flow velocity.

These turbulence properties are more intuitive to understand and can more easily be related to the physical characteristics of the problems. The values of I_T and L_T are not exactly known, but they can be estimated following some guidelines from the literature [12].

$$I_T = I Re_{D_h}^{-1/8} \quad (9)$$

$$L_T = l D_h \quad (10)$$

3 System Geometry

The system to be modelled is basically a linear pipe, where a pulp fibre suspension is flowing. Experimental tests with four industrial kinds of pulp fibre suspensions (recycled pulp, eucalypt bleached kraft pulp, pine unbleached kraft pulp and eucalypt (90%) + pine (10%) bleached kraft pulp, weight percentages) were performed in a pipe 4 m long and with 3 in of diameter (Figure (2)), supplying information about the pressure drop in the pipe for different conveying velocities. This is the geometry that has to be modelled and our parameter for comparison will be the pressure drop. Therefore, comparison of experimental versus predicted values can be made.

The model size was reduced in order to minimise the calculation time, without losing accuracy, by making use of 2D axial symmetry. Thus, a straight pipe, with a constant cross-sectional area can be reduced to a rectangular geometry in a 2D axisymmetric representation. Consequently, the modelled domain is simply a rectangle, the length corresponding to 1 m of pipe and the width to the 1.5 in (0.0381 m) radius.

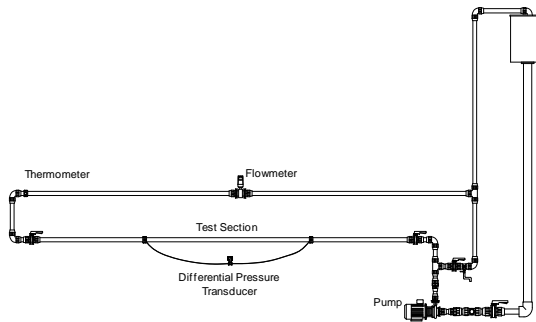


Figure 2: Schematic representation of the pilot rig [14].

3.1 Boundary conditions

Inlet boundary

The inlet fluid velocity was taken as a boundary condition, considering an uniform velocity profile in the pipe cross section.

Outlet boundary

The condition “Normal Stress, Normal Flow” was chosen to describe the outlet condition of the domain, since this condition determines that there must be no tangential velocities on the boundary.

Wall and symmetry boundaries

The wall boundary selected for the model must consider that turbulence close to a solid wall is very different from isotropic free-stream turbulence. To overcome this fact, an approach considering an empirical relation between the value of velocity and wall friction was introduced in the model. This relation known as “wall function” is accurate for high Reynolds numbers and in situations where pressure variations along the wall are not very large [7], which can be assumed in the case reported here. The wall boundary was modelled with a logarithm wall function; this wall function applied to finite elements assumes that the computation domain begins at a distance δ_w from the real wall. The logarithm wall function also assumes that the velocity vector is parallel to the wall.

The “Axial Symmetry” condition should be used on all boundaries with coordinate $r=0$

3.2 Discretization

In order to reach accurate results for the pressure drop, the mesh selected was a mapped mesh consisting of quadrilateral elements. This kind of mesh is structured in its pattern, and is recommended for geometries such that the domains are fairly regular in shape and do not contain holes, as is the case. The mesh is more refined near the wall to resolve the viscous sublayer.

3.3 Physical parameters settings

For the physical characterization of the system both density and viscosity needed to be introduced. For each pulp suspension, these values were collected experimentally. The density was measured by picnometry, while the viscosity was determined using a rotational viscometer specially designed to study fibrous systems [10]. Since the pulp fibre suspensions are clearly non-Newtonian fluids, the viscosity values were introduced on the model as

function of velocity. According to Wazer the apparent viscosity of a non-Newtonian fluid is defined as the ratio of the total shearing stress to the total rate of shear at a given value of shear rate [15]. It represents the viscosity of a Newtonian liquid exhibiting the same resistance to flow at a chosen shearing stress or shear rate. Mathematically:

$$\nu_{app} = \frac{\tau}{\dot{\gamma}} \quad (11)$$

where τ is the shear stress and $\dot{\gamma}$ is the rate of shear. Figure (3) shows an example of the rheograms obtained for a mixture of pine and eucalypt fibres for different consistencies. The apparent viscosity was computed for each pulp suspension, considering the corresponding rheograms and using Eq. (11). The results are shown in Figure (4) for the same mixture of pine and eucalypt.

For each consistency the average rate of shear can be

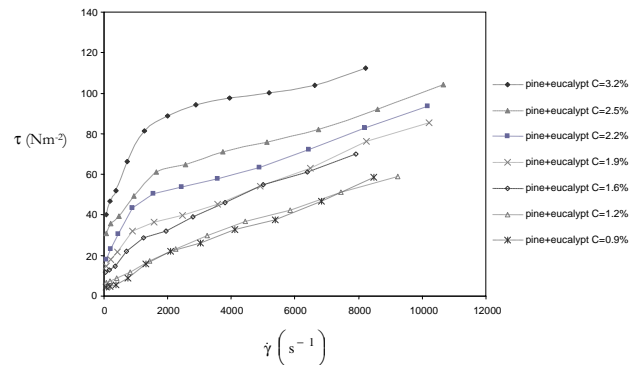


Figure 3: Rheograms for pine+eucalypt fibre suspensions.

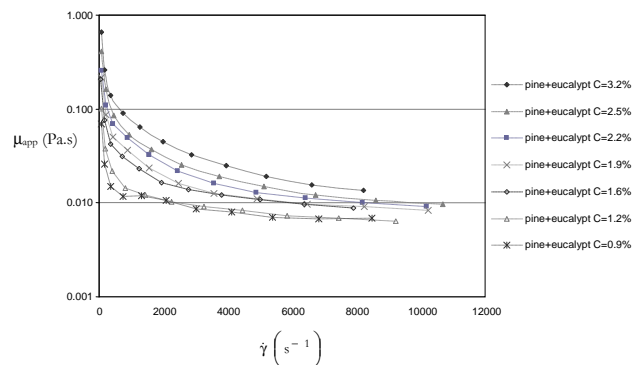


Figure 4: Apparent viscosity for the of pine+eucalypt fibres suspensions.

equated as a function of the tip speed of the rotor and introduced in the respective COMSOL model. Thus, the apparent viscosity can then be supplied as a function of local velocity. Flow correlations based on the pulp “viscosity” together with the fundamental equations of momentum balance can then be generated which can be used for the prediction of the friction factor and pressure drop in pipes.

Regarding the turbulence parameters, the I and l parameters values (Eq. (9) and Eq. (10)) for water flow are frequently assumed to be 0.16 and 0.07, respectively. It is well referenced in previous studies that the existence

of particles, such as fibres, in a fluid flow, induces a turbulence damping [1,2,8,16], which is reflected on the turbulence parameters decrease. Thus, the I and l values should be smaller than usually assumed for homogeneous fluids. However, the turbulence damping degree and, hence, the I and l variation are not exactly known. For pulp fibre suspensions it is expectable that the damping effect will depend on fibre type and on consistency.

Taking into account the aforementioned discussion, and in order to simulate the turbulence damping for both the I and l values of the modelling Eq. (9) and Eq. (10), smaller values than usually used for homogeneous fluids were introduced in the model. Since the turbulence length scale is mentioned to be mainly dependent on the system geometry, the l value was assumed to be constant, equal to 0.005, for all the fibre types and consistencies. The I parameter was adjusted according to the pulp fibre type and concentration.

4 Results

Firstly, the numerical implementation was validated with water, considering the water physical characteristics. Then, the pulp's physical characteristics were introduced in the model. It was considered that the suspensions start to flow in fully developed turbulence at velocities above the maximum of the drag reduction effect (V_{red}).

Table (2) summarizes the characteristics of the pulp suspensions tested, for which simulations were, simultaneously, conducted. As an example of an output result, Figure (5) shows the simulated pressure drop along 1 m of pipe for the case of the recycled pulp suspension with 2.7% (w/w) consistency, at a velocity of 4.8 m/s. As expected, simulation shows pressure decreasing along the pipe and, since the system is highly turbulent, the radial velocity profile is almost flat, remaining constant along the pipe because fully developed turbulent flow was assumed. The model's pressure drop results for each con-

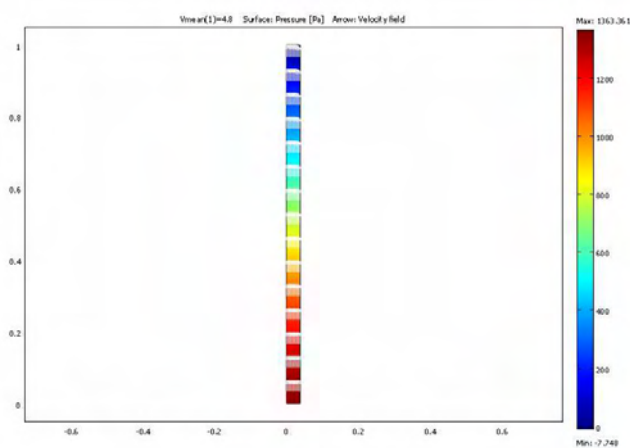


Figure 5: Output of the CFD code (COMSOL 3.4) for the recycled pulp suspension with 2.7% (w/w) consistency at a velocity of 4.8 m/s.

sistency and pulp type were compared with the experimental values, and the model's turbulence parameters were adjusted until a good fit with the experimental results was obtained. An example is shown in Figure (6) for two different consistencies of the pine pulp suspension.

From the many simulations performed for the different pulps and consistencies, the turbulence parameters

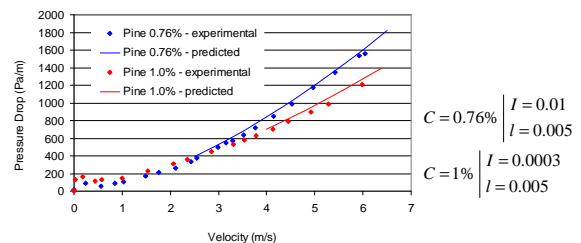


Figure 6: Experimental and predicted pressure drop for pine pulp suspensions at 0.76% and 1.0% consistency (C) in the turbulent regime.

values reported in Table (3) were found to be adequate for use at the several flow conditions.

From Table (3) it can be easily concluded that for very low consistencies the I value is minimally influenced by the increase in consistency, this meaning that a slight consistency variation for this range does not modify the turbulent flow mechanisms. Contrarily, for relatively high values of consistency it is observed that as the consistency increases the I values decrease for all the pulps. This trend was expected, since the presence of solids has an increasing damping effect on the longitudinal turbulence intensity, in agreement with previous studies [14]. Considering the unique characteristics of pulp fibre suspensions, whose components are able to develop new "suspension structures" it can be easily understood the large decrease of the I value, since these structures, which are not only bigger but also of a different nature, must modify the suspension turbulence characteristics. The highest turbulence damping was observed for the pine fibre suspension, followed by the eucalypt+pine and the eucalypt pulp suspensions. This fact is certainly related with both the fibres length and the fibres morphological characteristics. Pine fibres are the longest and stiffest ones. Regarding the recycled pulp suspension the effect of consistency was not so important. In fact, this different behaviour had already been recognised in other situations, such as in the rheological and flow behaviours [11,14]. In Figure (7) a comparison between the experimental data and the modelling results for the flow conditions tested (different pulps and consistencies) is made.

The predicted values for the pressure drop in pipes are very similar to the experimental ones. Regarding the lowest values of pressure drop for the fresh pulp fibre suspensions, a more careful observation shows that the simulation results are slightly over-predicted. These values correspond to the lowest flow velocities, so this difference can be due to the fact that at these velocities the turbulent flow regime may not be completely established. Considering the eucalypt fibre suspension (Figure (7) b)) the CFD model is not completely able to predict the pressure drop for the highest velocities: the calculated values are smaller than the experimental ones. These values correspond to the lowest consistencies at the highest velocities, and the observed trend may be due to the experimental rheological values used. In fact, due to limitations of the rheometer, very high shear velocities were impossible to reach and these values had to be extrapolated from the rheograms.

Pulp suspension	Recycled	Eucalyptus	Pine+Eucalyptus	Pine
Fibre length (mm)	1.14 ± 0.04	0.71 ± 0.03	0.61 ± 0.06	2.56 ± 0.14

Table 2: Length weighted mean fibre length of the pulp fibre suspensions

Pulp Type	Turbulence parameters	very low consistencies		low consistencies			
		Consistency (%)	0.72	0.61	1.40	1.80	2.30
Recycled	I	0.01	0.01	0.009	0.008	0.007	0.005
	l	0.005	0.005	0.005	0.005	0.005	0.005
	Consistency (%)	0.77	0.91	1.4	1.5		
Eucalypt	I	0.09	0.09	0.007		0.003	
	l	0.005	0.005	0.005		0.005	
	Consistency (%)	0.71	0.77	0.9	1.2	1.3	
Eucalypt+pine	I	0.07	0.05	0.01	0.005	0.003	
	l	0.005	0.005	0.005	0.005	0.005	
	Consistency (%)	0.66	0.76	0.8		1	
Pine	I	0.01	0.01	0.0005		0.0005	
	l	0.005	0.005	0.005		0.005	

Table 3: Turbulence parameters values.

5 Conclusions

The pressure drop values for the flow of fibre suspensions in pipes in the turbulent flow regime, obtained using COMSOL Multiphysics Software, agree very well with the experimental results obtained in a pilot rig. The use of the $k - \epsilon$ Turbulence Model for the simulation of pulp fibre suspensions flow, associated with the rheological data acquired in a viscometer especially designed to study multiphase systems, revealed to be an adequate strategy to attain good prediction of pressure drop values for fibre suspensions flow. The values of the turbulence parameters used to adjust the model confirm previous studies where it was concluded that the existence of particles, such as fibres, in a fluid flow, induces a turbulence damping. It is clear that the turbulence intensity scale, I_T , which is a function of I , decreases with pulp consistency increase.

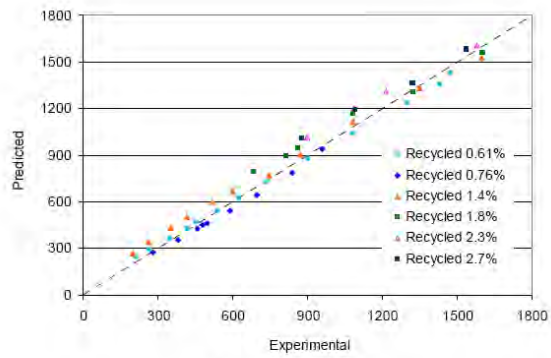
Acknowledgments

Acknowledgments are due to the EU project NODESZELOSS which supplied the financial support and to Prado Karton, GOPACA and CELTEJO, in Portugal, for supplying the pulps.

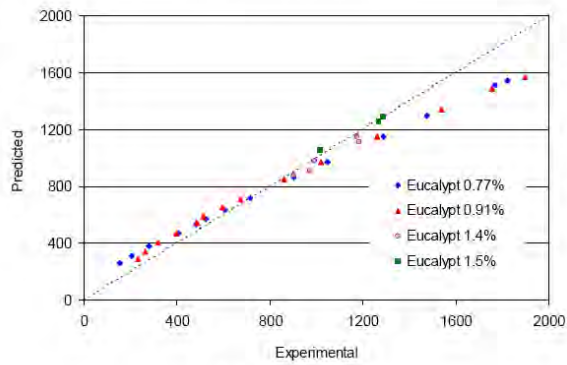
References

[1] Duffy, G.G. "Measurements, mechanisms and models: Some important insights into the mechanisms of flow of fibre suspensions".

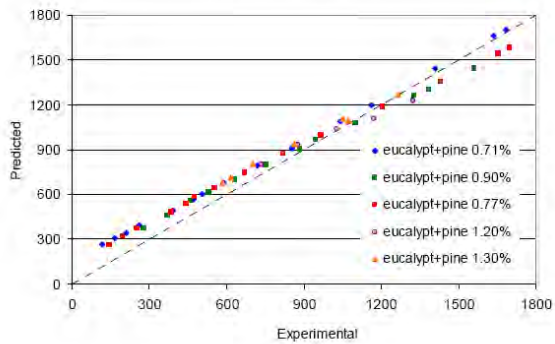
- Annual Transactions of the Nordic Rheology Society, 2006, 14.
- [2] Xu, H.J.; Aidun, C.K. "Characteristics of fiber suspension flow in a rectangular channel". Int. J. Multiphase Flow, 2005, 31, 318.
- [3] Moller, K. "General correlations of pipe friction data for pulp suspensions". Tappi J., 1976, 59, 111.
- [4] Duffy, G. G.; Titchener, A.L. "Design procedures for obtaining friction loss for chemical pulps". Tappi J., 1974, 57, 162.
- [5] Duffy, G.G.; Titchener, A.L; Moller, K. "The mechanisms of pulp suspensions in pipes". Appita Journal, 1976, 29, 363.
- [6] Moller, K. "A correlation of pipe friction data for paper suspensions". Ind. Eng. Chem., Process Des. Dev., 1976, 15, 16.
- [7] Duffy, G. G. "Flow of medium consistency wood pulp suspensions". Appita Journal, 1995, 48, 51.
- [8] Krochak, P. J.; Olson, J. A.; Martinez, D. M. "Fibre suspension flow in a tapered channel: the effect of flow/fibre coupling". Int. J. Multiphase Flow, 2009, 35, 678.
- [9] Cui, H.; Grace, J.R. "Flow of pulp fibre suspension and slurries: A review". Int. J. Multiphase Flow, 2007, 33, 921.
- [10] Blanco, A.; Negro, C.; Fuente, E.; Tijero, J. "Rotor selection for a Searl-type device to study the rheology of paper pulp suspensions". Chem. Eng. & Proc., 2007, 46, 37.
- [11] Ventura, C.A.F.; Blanco, A.; Negro, C.; Garcia, F.A.P.; Ferreira, P.; Rasteiro, M.G.. "Modelling Pulp Fibre Suspension Rheology". Tappi J, 2007, 6, 7, 17.
- [12] "Chemical Engineering Module User's Guide", COMSOL AB, Stockholm, Sweden, 2007.
- [13] Wilcox, D.C. "Turbulence Modelling for CFD", 2nd ed., DWC Industries, La Canada, California, 1998.
- [14] Ventura, C.A.; Garcia, F.a.p.; Ferreira, P.; Rasteiro, M.G. "Flow Dynamics of Pulp Fibre Suspensions". Tappi J., 2008, 7, 20.
- [15] Wazer, J.R.; Lyons, L.W.; Kim, K.Y.; Colewell, R.E. "Viscosity and Flow Measurement - A Laboratory Handbook of Rheology". Interscience Publishers, New York, 1963.
- [16] Zisselmar, R.; Molerus, O. "Investigation of solid-liquid pipe flow with regards to Turbulence Modification". The Chemical Engineering Journal, 1979, 18, 233.



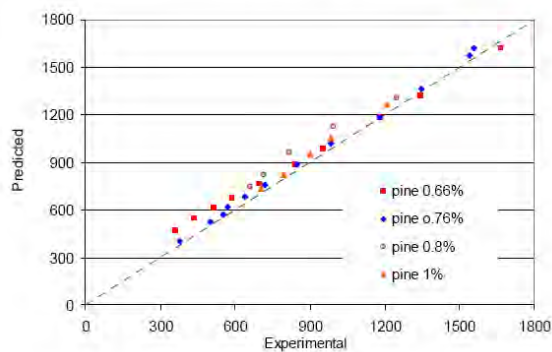
a) recycled



b) eucalypt



c) eucalypt+pine



d) pine

Figure 7: Comparison between the experimental pressure drop (Pa/m) and the modelling results for the flow conditions tested.

ERCOFTAC Special Interest Groups

1. Large Eddy Simulation

Geurts, B.J.
University of Twente, Holland.
Tel: +31 53 489 4125
Fax: +
b.j.geurts@math.utwente.nl

4. Turbulence in Compressible Flows

Comte, P.
University of Poitiers, France.
Tel: +33 5 49 36 60 11
Fax: +33 5 49 36 60 01
Pierre.comte@tea.univ-poitiers.fr

5. Environmental CFD

Morvan, H.
University of Nottingham, England.
Tel: +44 115 846 6374
Fax: +44 115 951 3898
herve.morvan@nottingham.ac.uk

10. Transition Modelling

Dick, E.,
University of Gent, Belgium.
Tel: +32 9 264 3301
Fax: +32 9 264 3586
erik.dick@ugent.be

12. Dispersed Turbulent Two Phase Flows

Sommerfeld, M.
Martin-Luther University, Germany.
Tel: +49 3461 462 879
Fax: +49 3461 462 878
martin.sommerfeld@iw.uni-halle.de

14. Stably Stratified and Rotating Flows

Redondo, J.M.
UPC, Spain.
Tel: +34 93 401 7984
Fax: +34 93 401 6090
Redondo@fa.upc.es

15. Turbulence Modelling

Jakirlic, S.
Darmstadt University of Technology,
Germany.
Tel: +49 6151 16 3554
Fax: +49 6151 16 4754
s.jakirlic@sla.tu-darmstadt.de

20. Drag Reduction and Flow Control

Choi, K-S.
University of Nottingham, England.
Tel: +44 115 9513 792
Fax: +44 115 9513 800
kwing-so-choi@nottingham.ac.uk

24. Variable Density Turbulent Flows

Anselmet, F.
IMST, France.
Tel: +33 4 91 505 439
Fax: +33 4 91 081 637
fabian.anselmet@irphe.univ-mrs.fr

28. Reactive Flows

Tomboulides, A.
Aristotle University of Thessaloniki,
Greece.
Tel: +30 2310 991 306
Fax: +30 2310 991 304
ananiast@enman.auth.gr

32. Particle Image Velocimetry

Stanislas, M.
Ecole Centrale de Lille, France.
Tel: +33 3 20 337 170
Fax: +33 3 20 337 169
stanislas@ec-lille.fr

33. Transition Mechanisms, Prediction and Control

Hanifi, A.
FOI, Sweden.
Tel: +46 8 5550 4334
Fax: +46 8 5550 3481
ardeshir.hanifi@foi.se

34. Design Optimisation

Giannakoglou, K.
NTUA, Greece.
Tel: +30 210 772 1636
Fax: +30 210 772 3789
kgianna@central.ntua.gr

35. Multipoint Turbulence Structure and Modelling

Cambon, C.
ECL Ecully, France.
Tel: +33 4 72 186 161
Fax: +33 4 78 647 145
claude.cambon@ec-lyon.fr

36. Swirling Flows

Braza, M.
IMFT, France.
Tel: +33 5 61 285 839
Fax: +33 5 61 285 899
braza@imft.fr

37. Bio-Fluid Mechanics

Van Steenhoven, A.A.
Eindhoven University of Technology,
Holland.
Tel: +31 40 2472 722
Fax: +31 40 2433 445
a.a.v.steenhoven@wtb.tue.nl

38. Microfluids and Micro Heat Transfer

Tardu, S.
Laboratoire des Ecoulements
Géophysiques et Industriels,
France.
sedat.tardu@hmg.inpg.fr

39. Aeroacoustics

Bailly, C.
Ecole Centrale de Lyon, France.
Tel: +33 4 72 186 014
Fax: +33 4 72 189 143
christophe.bailly@ec-lyon.fr

40. Smoothed Particle Hydrodynamics

Le Touzé, D.
Ecole Centrale de Nantes, France.
Tel: +33 2 40 37 15 12
Fax:
david.letouze@ec-nantes.fr

41. Fluid Structure Interaction

Longatte, E.
EDF, France.
Tel: +33 1 30 87 80 87
Fax: +33 1 30 87 77 27
elisabeth.longatte@edf.fr

42. Synthetic Models in Turbulence

Nicolleau, F.
University of Sheffield, England.
Tel: +44 114 22 27867
Fax: +44 114 22 27890
f.nicolleau@sheffield.ac.uk

43. Fibre Suspension Flows

Hämäläinen, J.
University of Kuopio, Finland.
Tel: +358 17 162279
Fax: +358 17 162585
jari.hamalainen@uku.fi

101. Quality and Trust in Industrial CFD

Hutton, A.G.
Airbus UK, England.
Tel: +44 117 936 7519
Fax:
anthony.hutton@airbus.com

102. ERCOFTAC Database Interests Group

Laurence, D.
UMIST, England.
Tel: +44 161 200 3704
Fax: +44 161 200 3723
dominique.laurence@manchester.ac.uk

ERCOFTAC Pilot Centres

Alpe – Danube – Adria

Reichl, C.
Austrian Institute of Technology,
Giefinggasse 2,
A-1210 Wien,
Austria.
Tel: +43 1 50550 6605
Fax: +43 1 50550 6439
christoph.reichl@arsenal.ac.at

Belgium

Geuzaine, P.
Cenaero,
CFD Multi-physics Group,
Rue des Frères Wright 29,
B-6041 Gosselies,
Belgium.
Tel: +32 71 919 334
philippe.geuzaine@cenaero.be

Czech Republic

Bodnar, T.
Institute of Thermomechanics AS CR,
5 Dolejskova,
CZ-18200 Praha 8,
Czech Republic.
Tel: +420 224 357 548
Fax: +420 224 920 677
bodnar@marian.fsik.cvut.cz

France – Henri Bénard

Cambon, C.
Ecole Centrale de Lyon.
LMFA,
B.P. 163,
F-69131 Ecully Cedex,
France.
Tel: +33 4 72 18 6161
Fax: +33 4 78 64 7145
claude.cambon@ec-lyon.fr

France South

Braza, M.
IMF Toulouse,
CNRS UMR – 5502,
Allée du Prof. Camille Soula 1,
F-31400 Toulouse Cedex,
France.
Tel: +33 5 61 28 5839
Fax: +33 5 61 28 5899
marianna.braza@imft.fr

France West

Bonnet, J-P.
Université de Poitiers,
Centre d'Etudes Aérodyn. et Thermiques,
43 Route de l'Aérodrome,
F-86036 Poitiers Cedex,
France.
Tel: +33 5 49 36 60 31
Fax: +33 5 49 45 60 01
jean-paul.bonnet@univ-poitiers.fr

Germany North

Gauger, N.
German Aerospace Center – DLR,
Institute of Aerodynamics,
Lilienthalplatz 7,
D-38108 Braunschweig,
Germany.
Tel: +49 531 295 3339
Fax: +49 531 295 2914
nicolas.gauger@dlr.de

Germany South

von Terzi, D.
Inst. Thermische Strömungsmaschinen,
Universität Karlsruhe (TH),
Kaiserstr. 12 (Geb. 10.91, Zi. 201)
D-76131 Karlsruhe,
Germany.
Tel: +49 721 608 6829
vonterzi@its.uni-karlsruhe.de

Germany West

Schröder, W.
RWTH – Aachen,
Institute of Aerodynamics,
D-52062 Aachen,
Germany.
Tel: +49 241 809 5410
Fax: +49 241 809 2257
ek@aia.rwth-aachen.de

Greece

Papailiou, K.D.
National Tech. University of Athens,
Laboratory of Thermal Turbomachines,
9 Iroon Polytechniou,
P.O. Box 64069,
Gr-15710 Athens, Greece.
Tel: +30 210 772 1634
Fax: +30 210 772 1658
kpapail@lft.ntua.gr

Iberian East

Onate, E.
Universitat Politecnica de Catalunya,
Edificio C-1, Campus Norte,
Gran Capitan s/n,
E-08034 Barcelona,
Spain.
Tel: +34 93 401 6035
Fax: +34 93 401 6517
onate@cimne.upc.es

Iberian West

Theofilis, V.
Universidad Politécnica de Madrid,
Plaza Cardenal Cisneros 3,
E-28040 Madrid,
Spain.
Tel: +34 91 336 3291
Fax: +34 91 336 6371
vassilis@torroja.dmt.upm.es

Italy

Martelli, F.
University of Florence,
Department of Energy,
Via Santa Marta 3,
I-50139 Firenze,
Italy.
Tel: +39 055 479 6237
Fax: +39 055 479 6342
francesco.martelli@unifi.it

Nordic

Wallin, S.
Swedish Defence Research Agency FOI,
Computational Physics,
S-16490 Stockholm,
Sweden.
Tel: +46 8 5550 3184
Fax: +46 8 5550 3062
stefan.wallin@foi.se

Poland

Drobnik, S.
Technical University of Czestochowa,
Thermal Machinery Institute,
Al. A. Krajowej 21,
PL-42200 Czestochowa,
Poland.
Tel: +48 34 325 0507
Fax: +48 34 325 0555
drobnik@imc.pcz.czyst.pl

Switzerland

Jenny, P.
ETH Zürich,
Institute of Fluid Dynamics,
Sonneggstrasse 3, ML H 38,
CH-8092 Zürich,
Switzerland.
Tel: +41 44 632 6987
Fax: +41 44 632 1147
jenny@ifd.mavt.ethz.ch

Netherlands

Ooms, G.
J.M. Burgerscentrum,
Research School for Fluid Mechanics,
Mekelweg 2,
NL-2628 CD Delft,
Netherlands.
Tel: +31 15 278 1176
Fax: +31 15 278 2979
g.ooms@wbmt.tudelft.nl

United Kingdom

Barton, I.
BAE Systems,
ATC – Sowerby, FPC 267,
P.O. Box 5,
Bristol BS34 7QW,
England.
Tel: +44 117 302 8251
Fax: +44 117 302 8007
iain.barton@baesystems.com



Best Practice Guidelines for Computational Fluid Dynamics of Dispersed Multi-Phase Flows

Editors

Martin Sommerfeld, Berend van Wachem
&
René Oliemans

The simultaneous presence of several different phases in external or internal flows such as gas, liquid and solid is found in daily life, environment and numerous industrial processes. These types of flows are termed multiphase flows, which may exist in different forms depending on the phase distribution. Examples are gas-liquid transportation, crude oil recovery, circulating fluidized beds, sediment transport in rivers, pollutant transport in the atmosphere, cloud formation, fuel injection in engines, bubble column reactors and spray driers for food processing, to name only a few. As a result of the interaction between the different phases such flows are rather complicated and very difficult to describe theoretically. For the design and optimisation of such multiphase systems a detailed understanding of the interfacial transport phenomena is essential. For single-phase flows Computational Fluid Dynamics (CFD) has already a long history and it is nowadays standard in the development of air-planes and cars using different commercially available CFD-tools.

Due to the complex physics involved in multiphase flow the application of CFD in this area is rather young. These guidelines give a survey of the different methods being used for the numerical calculation of turbulent dispersed multiphase flows. The Best Practice Guideline (BPG) on Computational Dispersed Multiphase Flows is a follow-up of the previous ERCOFTAC BPG for Industrial CFD and should be used in combination with it. The potential users are researchers and engineers involved in projects requiring CFD of (wall-bounded) turbulent dispersed multiphase flows with bubbles, drops or particles.

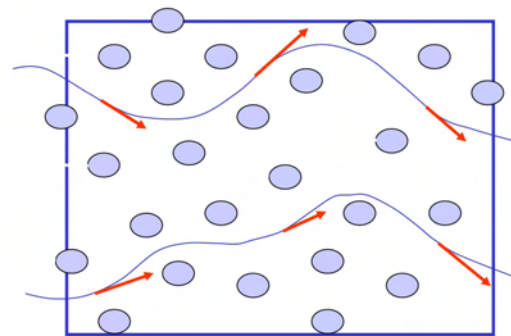


Table of Contents

1. Introduction
2. Fundamentals
3. Forces acting on particles, droplets and bubbles
4. Computational multiphase fluid dynamics of dispersed flows
5. Specific phenomena and modelling approaches
6. Sources of errors
7. Industrial examples for multiphase flows
8. Checklist of '*Best Practice Advice*'
9. Suggestions for future developments

* * *

Copies of the Best Practice Guidelines can be acquired electronically from the website:

www.ercoftac.org

Or from:

ERCOFTAC ADO
Chaussée de la Hulpe 187-189
B-1170 Brussels, Belgium
Tel: +32 2 643 3572, Fax: +32 2 647 9398
Email: emilie.jean@numeca.be

The price per copy is €90, €45 and €30 for ERCOFTAC industry, academic-and student members, respectively; and €180 for non-members.